



HAL
open science

Functional heterogeneity of POMC neurons relies on mTORC1 signaling

Nicolas Saucisse, Wilfrid Mazier, Vincent Simon, Elke Binder, Caterina Catania, Luigi Bellocchio, Roman Romanov, Stéphane Léon, Isabelle Matias, Philippe Zizzari, et al.

► To cite this version:

Nicolas Saucisse, Wilfrid Mazier, Vincent Simon, Elke Binder, Caterina Catania, et al.. Functional heterogeneity of POMC neurons relies on mTORC1 signaling. Cell Reports, 2021, 37 (2), pp.109800. 10.1016/j.celrep.2021.109800 . hal-03613014

HAL Id: hal-03613014

<https://hal.inrae.fr/hal-03613014>

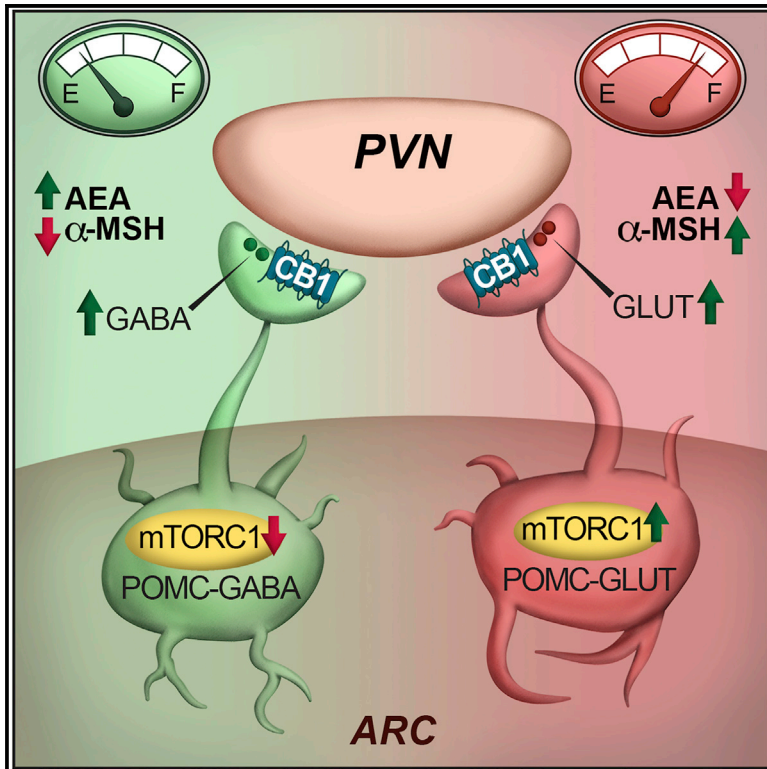
Submitted on 18 Mar 2022

HAL is a multi-disciplinary open access archive for the deposit and dissemination of scientific research documents, whether they are published or not. The documents may come from teaching and research institutions in France or abroad, or from public or private research centers.

L'archive ouverte pluridisciplinaire **HAL**, est destinée au dépôt et à la diffusion de documents scientifiques de niveau recherche, publiés ou non, émanant des établissements d'enseignement et de recherche français ou étrangers, des laboratoires publics ou privés.

Functional heterogeneity of POMC neurons relies on mTORC1 signaling

Graphical abstract



Authors

Nicolas Saucisse, Wilfrid Mazier, Vincent Simon, ..., Federico Massa, Giovanni Marsicano, Daniela Cota

Correspondence

daniela.cota@inserm.fr

In brief

Hypothalamic POMC neurons typically inhibit food intake. Saucisse et al. demonstrate that these neurons may have opposite effects on feeding depending on the neurotransmitter they release and that their function is coordinated by the mTORC1 kinase, which matches peptidergic- and neurotransmitter-dependent responses of POMC neurons to energy availability.

Highlights

- mTORC1 activity in POMC neurons controls food intake
- POMC neurons encompass heterogeneous cell subpopulations
- mTORC1 coordinates opposite POMC GABAergic and glutamatergic neuron responses
- POMC GABAergic and glutamatergic cells have distinct spatial and molecular features



Article

Functional heterogeneity of POMC neurons relies on mTORC1 signaling

Nicolas Saucisse,^{1,8} Wilfrid Mazier,^{1,8} Vincent Simon,^{1,8} Elke Binder,¹ Caterina Catania,¹ Luigi Bellocchio,¹ Roman A. Romanov,² Stéphane Léon,¹ Isabelle Matias,¹ Philippe Zizzari,¹ Carmelo Quarta,¹ Astrid Cannich,¹ Kana Meece,³ Delphine Gonzales,¹ Samantha Clark,¹ Julia M. Becker,⁴ Giles S.H. Yeo,⁴ Xavier Fioramonti,⁵ Florian T. Merkle,^{4,6} Sharon L. Wardlaw,³ Tibor Harkany,^{2,7} Federico Massa,¹ Giovanni Marsicano,¹ and Daniela Cota^{1,9,*}

¹University of Bordeaux, INSERM, Neurocentre Magendie, U1215, F-3300 Bordeaux, France

²Department of Molecular Neurosciences, Center for Brain Research, Medical University of Vienna, A-1090 Vienna, Austria

³Department of Medicine, Columbia University College of Physicians and Surgeons, New York, NY 10032, USA

⁴Medical Research Council (MRC) Metabolic Diseases Unit, University of Cambridge Metabolic Research Laboratories, Wellcome Trust-MRC Institute of Metabolic Science, Addenbrooke's Hospital, Cambridge CB2 0QQ, UK

⁵NutriNeuro, UMR 1286 INRAE, Bordeaux University, Bordeaux INP, F-33000 Bordeaux, France

⁶Wellcome Trust-MRC Cambridge Stem Cell Institute, Cambridge Biomedical Campus, Puddicombe Way, Cambridge CB2 0AW, UK

⁷Department of Neuroscience, Karolinska Institutet, SE-17177 Stockholm, Sweden

⁸These authors contributed equally

⁹Lead contact

*Correspondence: daniela.cota@inserm.fr

<https://doi.org/10.1016/j.celrep.2021.109800>

SUMMARY

Hypothalamic pro-opiomelanocortin (POMC) neurons are known to trigger satiety. However, these neuronal cells encompass heterogeneous subpopulations that release γ -aminobutyric acid (GABA), glutamate, or both neurotransmitters, whose functions are poorly defined. Using conditional mutagenesis and chemogenetics, we show that blockade of the energy sensor mechanistic target of rapamycin complex 1 (mTORC1) in POMC neurons causes hyperphagia by mimicking a cellular negative energy state. This is associated with decreased POMC-derived anorexigenic α -melanocyte-stimulating hormone and recruitment of POMC/GABAergic neurotransmission, which is restrained by cannabinoid type 1 receptor signaling. Electrophysiology and optogenetic studies further reveal that pharmacological blockade of mTORC1 simultaneously activates POMC/GABAergic neurons and inhibits POMC/glutamatergic ones, implying that the functional specificity of these subpopulations relies on mTORC1 activity. Finally, POMC neurons with different neurotransmitter profiles possess specific molecular signatures and spatial distribution. Altogether, these findings suggest that mTORC1 orchestrates the activity of distinct POMC neurons subpopulations to regulate feeding behavior.

INTRODUCTION

Food intake is controlled by the coordinated action of specialized brain cell types organized in specific networks. Within the arcuate nucleus (ARC) of the hypothalamus, two neuronal populations respectively expressing pro-opiomelanocortin (POMC) and Agouti-related peptide (AgRP) oppositely control food intake as a result of antagonistic effects on the central melanocortin receptors type 4 (MC4R) (Krashes et al., 2016).

POMC and AgRP neurons respond to nutrient and hormonal signals reflecting changes in energy availability (Cota et al., 2007; Krashes et al., 2016). Energy deficit activates AgRP neurons, which drive food seeking and intake through the release of the MC4R antagonist AgRP, the neuropeptide Y (NPY), and the inhibitory neurotransmitter γ -aminobutyric acid (GABA) (Tong et al., 2008). Conversely, energy surfeit activates POMC neurons, which typically promote satiety by releasing the

MC4R agonist α -melanocyte-stimulating hormone (α -MSH) (Krashes et al., 2016). Food intake after a prolonged fast, or re-feeding, increases POMC neurons activity, regulating meal size through α -MSH-dependent activation of MC4R in the hypothalamic paraventricular nucleus (PVN), among other brain areas (Balthasar et al., 2005; Fekete et al., 2012; Singru et al., 2007). However, the classic view of AgRP and POMC neurons as “Yin and Yang” partners regulating food intake through their opposite action on MC4R may be only a partial depiction of the relevant circuit. As recently suggested, AgRP neurons seem relevant for the search rather than the intake of food, while POMC neurons may be the ones controlling the whole feeding sequence, from its start to its termination (Brandt et al., 2018; Chen et al., 2015). In support of this hypothesis, POMC cleavage not only produces α -MSH but also the opioid β -endorphin, which stimulates food intake (Koch et al., 2015; Wardlaw, 2011). Besides, and differently from AgRP neurons, which are almost exclusively



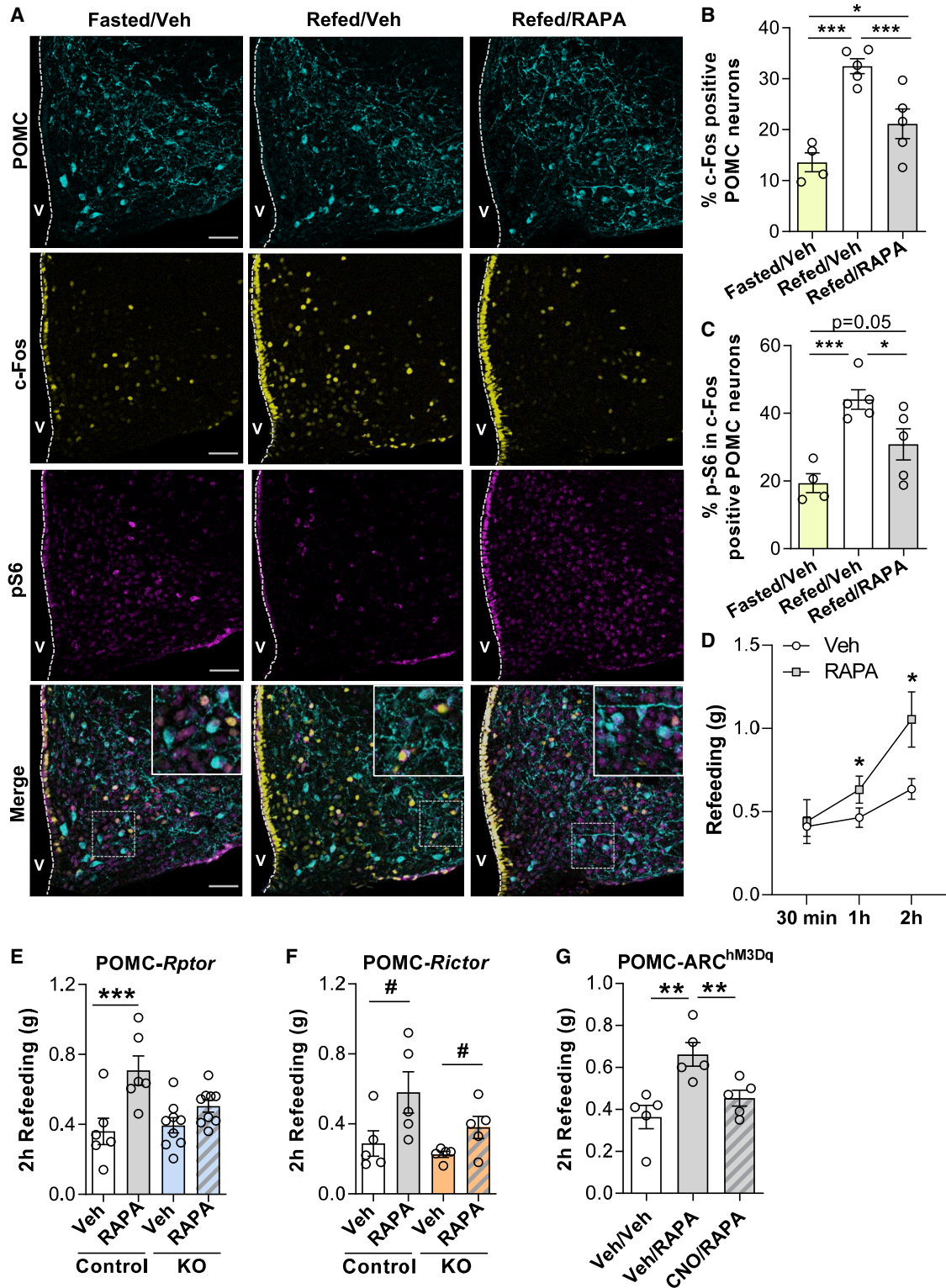


Figure 1. mTORC1 in POMC neurons controls food intake

(A–C) Representative images (A) and related quantification of c-Fos (B) and p-S6 (C) labeling in POMC-positive neurons in the ARC of C57BL/6 mice 24 h fasted or 90 min refed treated i.c.v. with rapamycin (RAPA) or its vehicle (n = 4–5 mice per group).

(D) Refeeding of C57BL/6 mice treated i.c.v. with RAPA or its vehicle (n = 5 mice per group).

(legend continued on next page)

GABAergic (Tong et al., 2008), POMC neurons include GABAergic and glutamatergic cells, as well as neurons containing both or neither of these neurotransmitters (Dicken et al., 2012; Hentges et al., 2004, 2009; Mazier et al., 2019; Wittmann et al., 2013). Finally, recent single-cell transcriptomic studies have revealed that POMC neurons are molecularly heterogeneous (Campbell et al., 2017; Henry et al., 2015; Lam et al., 2017). Thus, understanding how the specific roles of molecularly identified POMC neurons subpopulations are integrated to regulate food intake remains an important challenge.

The mechanistic target of rapamycin (mTOR) kinase is a cellular energy sensor, whose increased activity is a readout of positive energy availability (Haissaguerre et al., 2014). By forming two distinct complexes (mTOR complex 1 [mTORC1] and mTOR complex 2 [mTORC2]), mTOR controls cellular responses to nutrients, growth factors, hormones, and stress (Haissaguerre et al., 2014). In neurons, the mTOR pathway regulates soma size and dendrite and axon growth (Bockaert and Marin, 2015), and it affects both glutamatergic and GABAergic transmission (Weston et al., 2012). mTORC1 signaling participates in the regulation of energy balance by modulating the function of AgRP and POMC neurons (Burke et al., 2017; Cota et al., 2006; Dagon et al., 2012; Smith et al., 2015). mTORC1 also regulates oxidative metabolism in POMC neurons (Haissaguerre et al., 2018) and POMC/glutamatergic transmission in the PVN (Mazier et al., 2019). However, it is unknown whether mTORC1 signaling may exert a differential role depending on the neurotransmitter nature of the POMC neurons under its control.

GABAergic and glutamatergic transmission is regulated by multiple and specific mechanisms (Dietrich and Horvath, 2013). Among these, the retrograde suppression of neurotransmitter release through endocannabinoids acting at the presynaptic cannabinoid type 1 receptor (CB₁R) is well-known (Busquets-Garcia et al., 2018). Brain CB₁R activation generally stimulates food intake (Mazier et al., 2015), and it offsets α -MSH effects, particularly in the PVN (Mazier et al., 2019; Monge-Roffarello et al., 2014; Verty et al., 2004). However, the impact of brain CB₁R on food intake is also cell type specific. Indeed, although CB₁R-dependent inhibition of glutamatergic transmission induces hyperphagia, CB₁R-dependent inhibition of GABAergic neurons promotes hypophagia (Bellocchio et al., 2010; Soria-Gómez et al., 2014b). Whether CB₁R on POMC neurons might affect feeding by modulating GABA or glutamate release from these cells is unknown.

Here we used multiple approaches to address the role of the mTORC1 pathway in modulating the activity of POMC neurons and the associated feeding response. These studies have revealed functionally distinct POMC neurons subtypes, whose activity is under the control of mTORC1 and CB₁R signaling. These findings pinpoint specific molecular mechanisms engaged by

different POMC neurons subpopulations to oppositely regulate feeding and suggest that one physiological purpose of the mTORC1 pathway is to coordinate both neuropeptidergic- and neurotransmitter-dependent responses of POMC neurons in relation to changes in energy availability. Altogether, this evidence challenges classic notions about the role of POMC neurons as exclusive drivers of satiety.

RESULTS

mTORC1 signaling in POMC neurons regulates food intake

Detection of energy availability by POMC neurons is essential for their ability to regulate food intake (Cota et al., 2007; Krashes et al., 2016). Among the possible molecular mechanisms involved, mTORC1 activity is known to be a cellular readout of energy availability (Haissaguerre et al., 2014).

To test the relevance of the mTORC1 pathway in modulating POMC neuronal function and food intake, we acutely inhibited mTORC1 activity by delivering the mTORC1 inhibitor rapamycin (RAPA), which mimics a state of low energy availability in cells (Haissaguerre et al., 2014). The drug was given intracerebroventricularly (i.c.v.) just before allowing 24-h fasted mice access to food, because it is known that refeeding activates POMC neurons (Baithasar et al., 2005; Fekete et al., 2012; Singru et al., 2007). As expected, increased expression of the neuronal activity marker c-Fos (Fekete et al., 2012; Singru et al., 2007) was observed in POMC neurons after 90 min of refeeding (Figures 1A–1C). This was accompanied by increased phosphorylation of the ribosomal S6 protein (p-S6), a downstream target of mTORC1 (Haissaguerre et al., 2014) (Figures 1A–1C). RAPA administration partly prevented c-Fos and p-S6 increases in POMC cells of refeed animals (Figures 1A–1C) and caused hyperphagia (Figure 1D).

To verify that acute mTORC1 inhibition in POMC neurons was involved in the RAPA-mediated effect on food intake, we used POMC-*Rptor*-KO (knockout) mice, which carry a POMC neuron-specific deletion of the gene *Rptor*, which is necessary for functional mTORC1 signaling (Haissaguerre et al., 2018; Hara et al., 2002). These animals have a modest increase in their unstimulated food intake (Haissaguerre et al., 2018). RAPA i.c.v. administration caused hyperphagia in POMC-*Rptor*-controls, but not in KO littermates (Figure 1E). In contrast, the drug increased food intake of mutant mice lacking the gene *Rictor* (required for mTORC2 formation; Sarbassov et al., 2004) in POMC neurons (POMC-*Rictor*-KO mice; Figures S1A and S1B) to a comparable level relative to their controls (Figure 1F). POMC-*Rictor*-KO mice also had unstimulated food intake similar to their controls (Figure S1C). Thus, acute pharmacological blockade of mTORC1 activity causes hyperphagia by targeting mTORC1 rather than mTORC2 in POMC neurons.

(E and F) 2-h refeeding of POMC-*Rptor*-control and KO littermates (E) (n = 6–9 mice per group), and POMC-*Rictor*-control and KO littermates (F) (n = 5 mice per group) treated i.c.v. with RAPA or its vehicle.

(G) Acute intraperitoneal (i.p.) CNO inhibits i.c.v. RAPA-induced 2-h hyperphagia in POMC-ARC^{hM3Dq} mice (n = 5 mice per group).

Data are mean \pm SEM and were analyzed by repeated measures (RM) two-way ANOVA (D–F), one-way ANOVA (B, C), or RM one-way ANOVA (G) followed by Fisher's least significant difference (LSD) post hoc test. *p < 0.05, **p < 0.01, ***p < 0.001; #p < 0.05, treatment effect. Scale bars: 50 μ m (A); 10 μ m (A, smaller insets). V, 3rd ventricle. See also Figure S1 and Table S3.

To further explore whether POMC neurons activity played a necessary role for RAPA-induced hyperphagia, we analyzed the effects of mTORC1 inhibition in mice whereby POMC neurons were activated using a designer-receptors-exclusively-activated-by-designer-drugs (DREADD) approach (Alexander et al., 2009). The gene encoding the evolved human M3-muscarinic receptor fused to the fluorescent protein mCherry (hM3Dq-mCherry) was selectively expressed in POMC neurons by a Cre-inducible adeno-associated viral vector (AAV-DIO-hM3Dq-mCherry) injected into the ARC of POMC-Cre mice (Balthasar et al., 2004) to obtain POMC-ARC^{hM3Dq} animals (Zhan et al., 2013). As expected, systemic administration of the hM3Dq ligand clozapine-N-oxide (CNO; 1 mg/kg) increased the expression of c-Fos in mCherry-expressing POMC neurons, demonstrating efficient activation (Figures S1D and S1E). c-Fos-positive cells largely co-expressed the mTORC1 downstream target p-S6 (Figures S1D and S1F). Repeated daily administration of CNO over several days decreased food intake (data not shown), as in Zhan et al. (2013). Conversely, and in agreement with Koch et al. (2015) and Zhan et al. (2013), acute CNO injection did not alter food intake of POMC-ARC^{hM3Dq} mice (Figure S1G) but prevented the hyperphagic effect of RAPA (Figure 1G). CNO was unable to block RAPA-induced hyperphagia in POMC-ARC^{hM3Dq}-controls (not expressing Cre in POMC neurons; Figure S1H), showing that the drug had no effect per se (Gomez et al., 2017).

Hence acute mTORC1 inhibition increases food intake by likely decreasing POMC neurons activity, which led us to investigate whether changes in POMC-derived neuropeptides and/or neurotransmission were involved in this phenomenon.

Acute inhibition of mTORC1 activity causes fasting-like changes in the hypothalamic levels of α -MSH and endocannabinoids

POMC must be cleaved to generate active peptides that modulate food intake (Wardlaw, 2011). We measured the hypothalamic content of POMC and its processing intermediates and cleavage products in 24-h fasted and 2-h refeed mice treated i.c.v. with RAPA or vehicle. Neither POMC nor its initial product adrenocorticotrophic hormone (ACTH) was altered by RAPA or refeeding (Figures 2A and 2B). However, hypothalamic levels of α -MSH were increased after refeeding relative to fasting, and RAPA administration just before access to food prevented this increase (Figure 2C). α -MSH promotes satiety (Balthasar et al., 2005; Singru et al., 2007, 2012), whereas β -endorphin stimulates feeding (Koch et al., 2015). The latter, however, did not show significant changes in response to refeeding or RAPA (Figure 2D). Thus, acute inhibition of mTORC1 activity favors hyperphagia by likely preventing the increase in hypothalamic α -MSH levels typically observed after food intake (Krashes et al., 2016).

Opposite to α -MSH, hypothalamic endocannabinoids levels are high in fasting and low in refeeding (Kirkham et al., 2002). Moreover, CB₁R activation counteracts behavioral and neuro-modulatory effects of α -MSH (Mazier et al., 2019; Monge-Roffarello et al., 2014; Verty et al., 2004), which led us to posit the existence of a reciprocal relation between α -MSH and endocannabinoid regulation in response to mTORC1 modulation. As compared with fasting, refeeding dampened hypothalamic

levels of the endocannabinoid anandamide (AEA) (Figure 2E). However, i.c.v. administration of RAPA just before access to food prevented the decrease of AEA, maintaining its hypothalamic levels high, like in fasting (Figure 2E). RAPA had no effect on the hypothalamic (Figure 2F) or extra-hypothalamic (Table S1) content of the other endocannabinoid 2-arachidonoyl glycerol (2-AG) or on extra-hypothalamic levels of AEA (Table S1). Thus, acute blockade of mTORC1 activity causes opposite changes in hypothalamic α -MSH and AEA levels, which are associated with hyperphagia.

mTORC1-dependent recruitment of CB₁R signaling restrains GABA release from POMC neurons

To determine whether RAPA-induced increase in food intake was due to recruitment of endocannabinoid-CB₁R signaling, a sub-anorectic dose of the CB₁R antagonist rimonabant was simultaneously administered i.c.v. with RAPA. Rimonabant fully blocked the effect of RAPA on food intake (Figure S2A). Likewise, i.c.v. RAPA caused hyperphagia in controls, but not in whole-body CB₁-KO littermates, who lack the *Cnr1* gene (also known as CB₁) (Figure S2B). Thus, acute blockade of mTORC1 activity requires increased endocannabinoid-CB₁R signaling to modulate food intake. To determine whether this response was due to CB₁R signaling in POMC neurons, we evaluated the effect of RAPA in mice lacking CB₁ in these neuronal cells (POMC-CB₁-KO mice; Mazier et al., 2019). Deletion of CB₁ from POMC neurons did not alter 24-h food intake (Figure S2C) or the refeeding response (Figure 3A). As expected, i.c.v. RAPA administration just before access to food caused hyperphagia in POMC-CB₁-controls (Figure 3A). Surprisingly, however, POMC-CB₁-KO mice displayed even greater hyperphagia than their controls in response to the drug (Figure 3A). This implies that CB₁R signaling on POMC neurons might inhibit food intake in response to acute changes in mTORC1 activity. We have previously shown that activation of CB₁R on GABAergic terminals decreases food intake (Bellocchio et al., 2010). Because POMC neurons can be GABAergic (Hentges et al., 2009), we hypothesized that RAPA-induced hyperphagia in POMC-CB₁-KO mice might depend on increased GABA release from POMC synaptic terminals. Confirming this hypothesis, co-administration of a sub-effective dose (0.03 μ g/ μ L i.c.v.; Figures S2D and S2E) of the GABA_A receptor antagonist picrotoxin (Ptx) prevented the enhanced response to RAPA in POMC-CB₁-KO mice (Figure 3A). To then confirm that lack of CB₁R on POMC neurons alters POMC/GABAergic transmission, we evaluated miniature inhibitory post-synaptic currents (mIPSCs) frequency onto parvocellular neurons of the PVN. This set of cells is one of the targets of POMC neurons for the control of food intake (Mazier et al., 2019; Singru et al., 2012). At one with the inhibitory role of CB₁R activation on neurotransmitter release (Busquets-Garcia et al., 2018), bath application of the CB₁R agonist WIN 55,212-2 inhibited mIPSCs frequency in controls, but not in POMC-CB₁-KO littermates (Figures 3B–3D), implying that endocannabinoid CB₁R-dependent inhibition of GABAergic transmission is lacking in POMC-CB₁-KO mice.

Thus, acute mTORC1 blockade may activate POMC/GABAergic transmission, thereby leading to increased food intake under the negative control of CB₁R signaling.

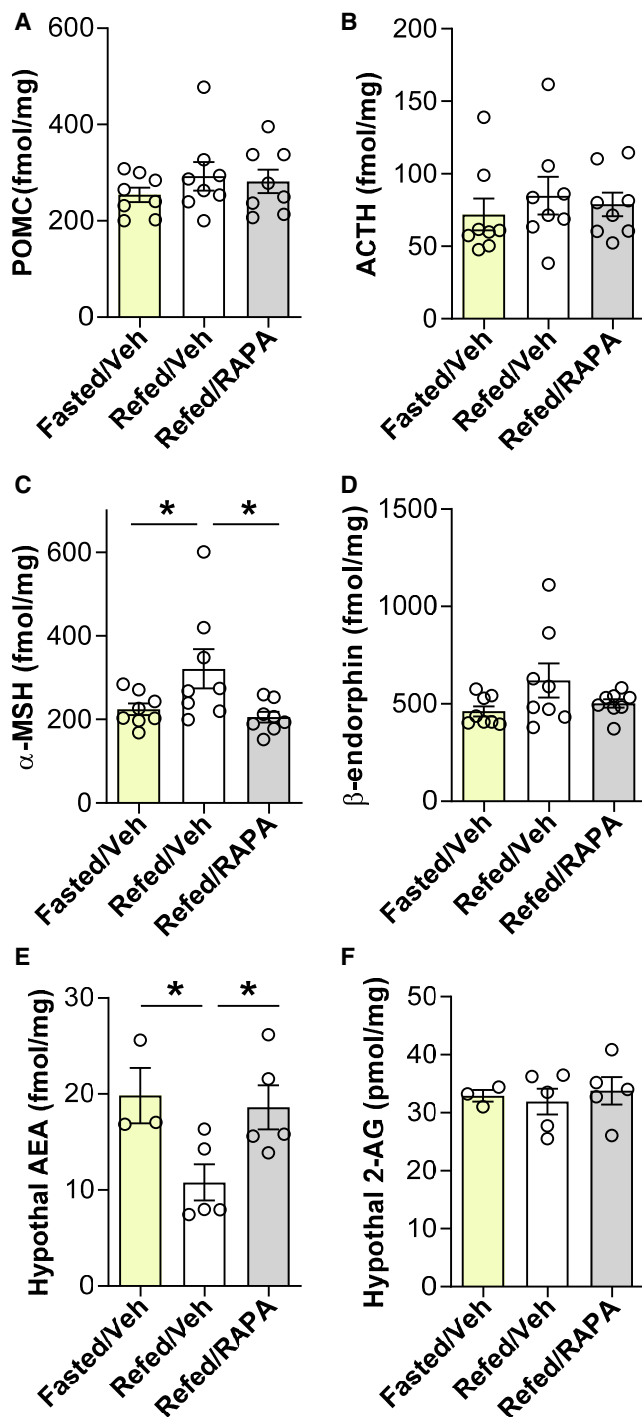


Figure 2. mTORC1 blockade induces fasting-like α -MSH and AEA changes in the hypothalamus

(A–F) Hypothalamic content of POMC (A), ACTH (B) α -MSH (C), β -endorphin (D), and the endocannabinoids AEA (E) and 2-AG (F) in fasted or refed C57BL/6 mice treated i.c.v. with RAPA or its vehicle (n = 8 mice per group for neuropeptides; 3–5 mice per group for endocannabinoids). Data are mean \pm SEM and were analyzed by one-way ANOVA followed by Fisher’s LSD post hoc test (A–F). *p < 0.05.

See also Tables S1 and S3.

mTORC1 activity oppositely regulates POMC/GABAergic and POMC/glutamatergic neurons

Based on this evidence, we then characterized the effect of RAPA on POMC neuronal firing activity in hypothalamic slices obtained from POMC-YFP mice. Taking all recorded cells together, RAPA had no effect on firing frequency (n = 117; Figure S3A). However, to assess cell-specific changes, we carried out an individual firing analysis by comparing the firing rate before and during RAPA application using normalization via Z score transformation of individuals’ instantaneous frequencies values (Courtin et al., 2014). This approach led to the identification of distinct POMC neuronal populations: (1) POMC neurons inhibited by RAPA (RAPA^{inh}; n = 41/117, 35.1%; Figures 4A and 4B), (2) POMC neurons activated by RAPA (RAPA^{act}; n = 37/117, 31.6%; Figures 4A and 4C), and (3) POMC neurons not responding to RAPA (RAPA^{ns}; n = 39/117, 33.3%; Figures 4A and 4D).

To then assess whether RAPA had an intrinsic action on POMC neurons, we repeated electrophysiology studies in the presence of synaptic blockers (Figure S3B). Under this condition, ~33% of POMC cells were still activated and ~16% were inhibited by RAPA, implying that RAPA directly activates some POMC neurons, while its inhibitory effect involves both direct and indirect actions.

Importantly, subpopulations of POMC cells differently responding to RAPA had specific electrophysiological characteristics, suggesting distinct functional properties. RAPA^{act} POMC neurons had higher membrane resting potential (Em) and resistance (Figures 4E and 4F) and lower membrane capacitance (Cm; Figure 4G) than RAPA^{inh} POMC cells, whereas RAPA^{ns} cells had intermediate characteristics (data not shown). RAPA oppositely modified the Em of RAPA^{act} and RAPA^{inh} POMC cells (Figure S3C). An inverse correlation was also found between the recorded cells’ Cm and the firing changes induced by RAPA (Figure 4H).

Thus, acute modulation of mTORC1 activity allows identifying POMC neurons with different electrophysiological properties. This may be true not only when inhibiting mTORC1 with RAPA but also when activating this pathway with the hormone leptin, which requires mTORC1 signaling in POMC neurons to decrease food intake (Cota et al., 2006; Dagon et al., 2012; Haissaguerre et al., 2018). As observed with RAPA, when taking into account all recorded POMC cells, leptin (200 nM) had no effect on firing frequency (n = 69; Figure S4A). However, individual firing analysis done by comparing the firing rate before and during leptin application allowed stratifying POMC neurons into three main subtypes: (1) POMC cells activated by leptin (n = 25/69, 36.2%; Figures S4B and S4C), (2) POMC cells inhibited by leptin (n = 20/69, 29%; Figures S4B and S4D), and (3) POMC cells not responding to leptin (n = 24/69, 34.8%; Figures S4B and S4E). Notably, electrophysiological characteristics of POMC cells activated and inhibited by leptin (Figures S4F–S4I) were comparable with those of cells respectively inhibited and activated by RAPA (Figures 4E–4H), suggesting that POMC neurons with similar electrophysiological characteristics oppositely respond to opposite signals of energy availability.

Cm is an indicator of cell size (Hentges et al., 2009), and the smaller size of POMC/GABAergic neurons relative to POMC/glutamatergic ones allows distinguishing these two neuronal subtypes (Hentges et al., 2004, 2009). Based on the

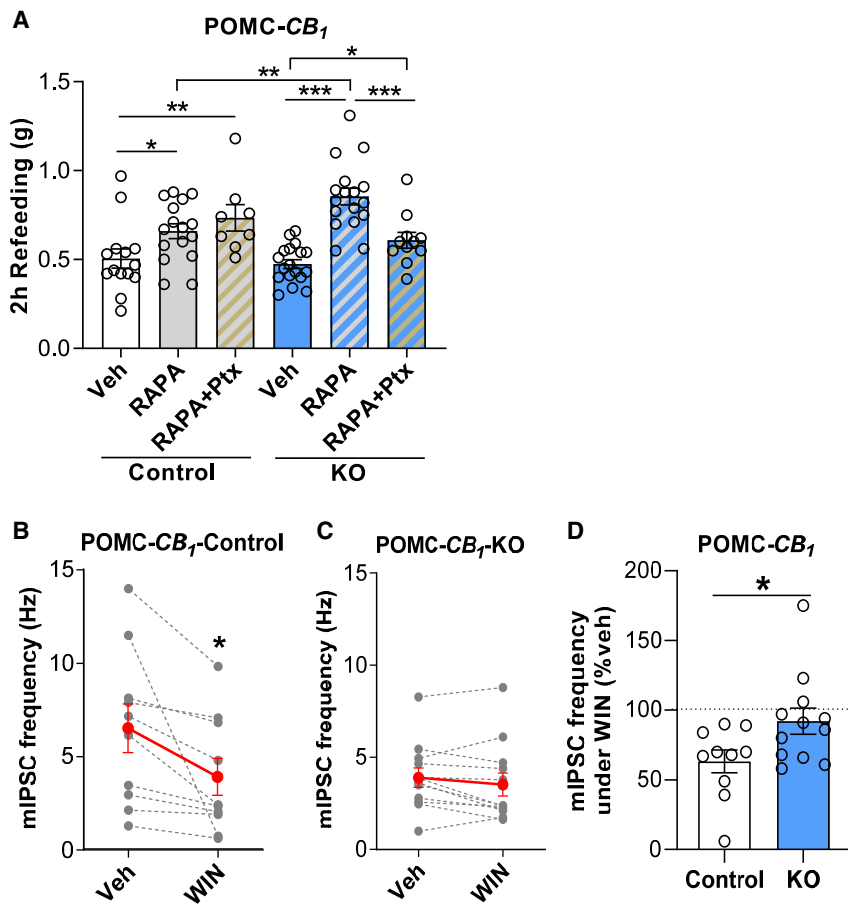


Figure 3. Role of CB₁R in POMC neurons in RAPA-induced hyperphagia

(A) Refeeding in POMC-CB₁-controls and -KO littermates treated i.c.v. with RAPA, its vehicle, or a combination of RAPA and the GABA_A receptor antagonist picrotoxin (Ptx) (n = 8–18 mice per group, 2 experiments combined together).

(B–D) Effect of the CB₁R agonist WIN55-212 on miniatures inhibitory post-synaptic currents (mIPSC) frequency of parvocellular neurons of the PVN of POMC-CB₁-control (B, n = 10 cells) and -KO littermates (C, n = 12 cells); (D) change in mIPSC frequency under WIN (n = 10–12 cells).

Data are mean ± SEM and were analyzed by two-way ANOVA followed by Fisher's LSD post hoc test (A), paired (B and C), and unpaired (D) t test. *p < 0.05, **p < 0.01, ***p < 0.001. See also Figure S2 and Table S3.

Cm, we hypothesized that RAPA^{inh} POMC cells were likely glutamatergic, while RAPA^{act} POMC neurons were GABAergic. Hence recorded neurons were filled with biocytin and labeled with an antiserum directed against the GABAergic markers GAD65/67. By using 3D image reconstruction analysis, RAPA^{act} POMC neurons had significant intracellular GAD65/67 staining, whereas RAPA^{inh} POMC neurons did not overcome background staining levels (Figures 4I, 4J, S3D and S3E). GAD65/67 staining positively correlated with the firing changes induced by RAPA (Figure 4K) and was inversely associated with the Cm of the analyzed cells (Figure S3F). A negative correlation was also found between the firing changes caused by RAPA and the Cm (Figure S3G), overall implying that small POMC cells activated by RAPA are likely GABAergic.

Then, by using optogenetics, we evaluated whether the acute inhibition of mTORC1 activity could alter POMC-driven neurotransmission. Using the FLEX system, we expressed the photoactivable channelrhodopsin-2 (ChR2) in POMC-Cre neurons (Atasoy et al., 2008) and recorded light-evoked ARC POMC synaptic inputs onto PVN parvocellular neurons (Figure 5A). About 1 in 10 parvocellular neurons were synaptically connected to terminals arising from infected POMC neurons (31/321 cells; 9.66%). Pharmacological assays on light-evoked synaptic transmission were performed in 17 parvocellular cells (Figures 5B and S5; Table S2). The majority of the POMC terminals connecting onto

parvocellular neurons were pure glutamatergic inputs (58.82%; 10/17), whereas the remaining recorded cells received pure GABAergic (17.65%; 3/17) or mixed GABA/glutamate inputs (23.53%; 4/17) (Figure 5B). To test the involvement of mTORC1 in the control of neurotransmitter release from POMC terminals onto parvocellular neurons, we challenged light-evoked neurotransmission by adding RAPA to the perfusate. Acute inhibition of mTORC1 activity reduced light-evoked excitatory post-synaptic currents (eEPSCs) amplitude (Figures 5C and 5D), while increasing light-evoked inhibitory post-synaptic currents (eIPSCs) amplitude (Figures 5C and 5E). Thus, mTORC1 activity oppositely regulates POMC/GABAergic and POMC/glutamatergic transmission.

POMC neurons with specific neurotransmitter profiles have distinct molecular fingerprints and spatial distribution

Finally, we characterized POMC neurons based on the neurotransmitter type they express. To this purpose, we aligned POMC neurons to GABA, glutamate, or mixed neurotransmitters expression, and we analyzed publicly available single-cell RNA sequencing (RNA-seq) data of POMC neurons from C57BL/6 mice (accession number GEO: GSE74672; Romanov et al., 2017) by means of differential expression profiling. POMC/GABAergic and POMC/glutamatergic subpopulations had non-overlapping gene expression profiles (Figures 6A and S6), while mixed GABAergic/glutamatergic cells expressed molecular markers typical of both POMC/GABAergic and POMC/glutamatergic neurons (Figures 6A and S6). Few POMC/GABAergic neurons also expressed the orexigenic neuropeptides *Npy* and *Agrp*, which was confirmed by fluorescent *in situ* hybridization (FISH) (Figure S7A). *Mtor*, *Rptor*, *Rictor*, and *CB₁* were detected in all POMC subpopulations (see GEO: GSE74672). Differential gene expression analysis done on POMC/GABAergic versus POMC/glutamatergic subpopulations revealed only the heterogeneous

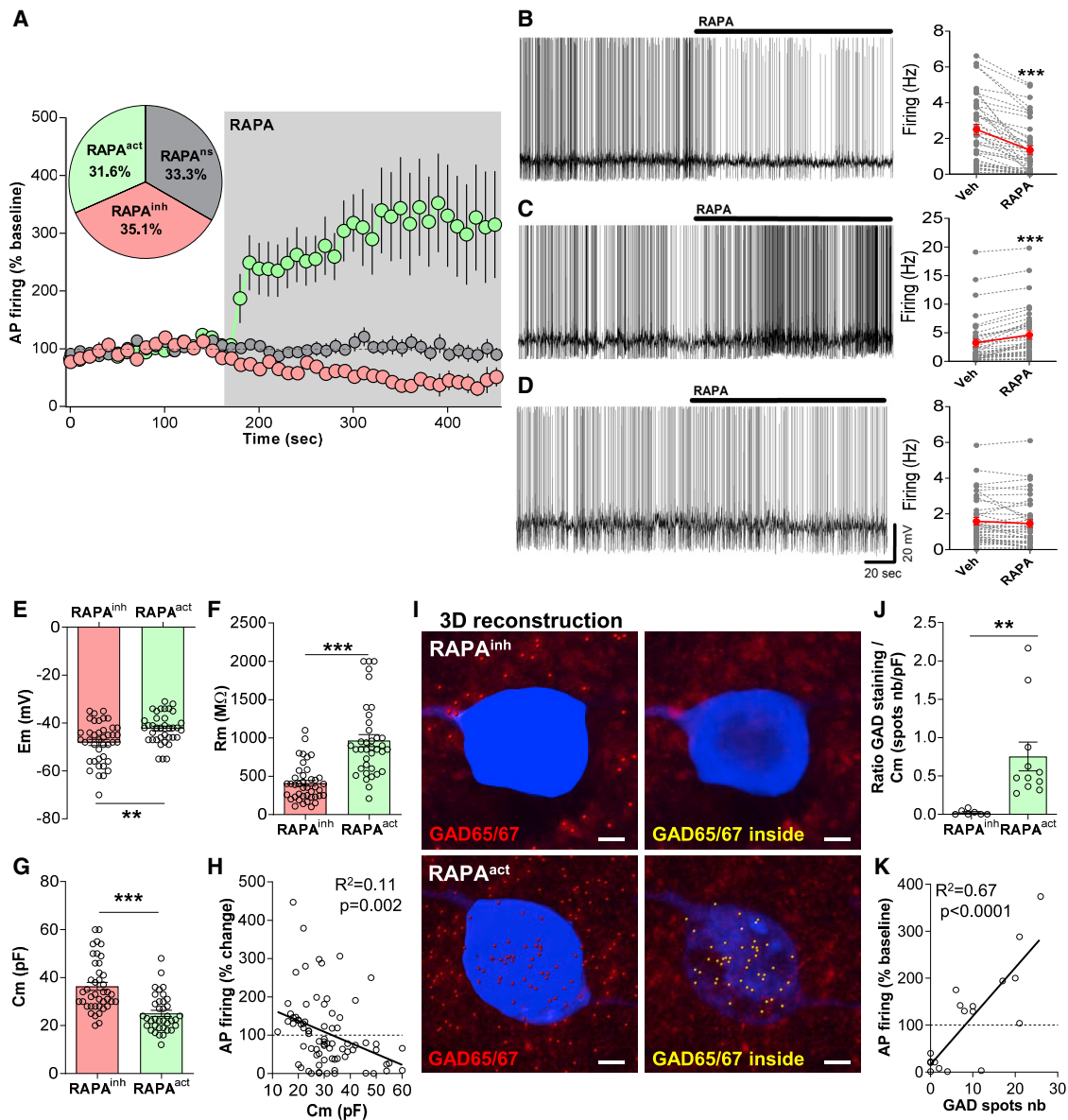


Figure 4. mTORC1 blockade oppositely regulates POMC neuron activity depending on neurotransmitter cell type

(A) Repartition of POMC neurons as a function of their response to RAPA (200 nM).

(B–D) Representative traces of POMC neurons firing during RAPA perfusion and corresponding firing changes in response to RAPA (right side). RAPA decreases (B, $n = 41/117$ cells), increases (C, $n = 37/117$ cells), or has no effect (D, $n = 39/117$ cells) on POMC firing (46 mice analyzed in total).

(E–G) RAPA^{act} POMC neurons ($n = 37$) have increased membrane resting potential (E_m ; E) and membrane resistance (R_m ; F) and decreased cell capacitance (C_m ; G) as compared with RAPA^{inh} POMC neurons ($n = 41$).

(H) Change in cell firing in response to RAPA is correlated with C_m ($n = 78$ cells).

(I) Representative 3D reconstruction from z stack confocal images of RAPA^{inh} and RAPA^{act} POMC neurons used for electrophysiological recordings. Reconstruction of cell body (biocytin: blue surface) and GAD staining (GAD65/67: red spots, left panel), and corresponding images showing only the GAD spots present inside the cell body surface (yellow, right panel).

(J) Number of GAD65/67 spots inside the cell surface over membrane capacitance is higher in RAPA^{act} POMC neurons as compared with RAPA^{inh} POMC neurons ($n = 7–11$ cells).

(K) Change in action potential firing under RAPA correlates with the number of GAD spots present inside the cell ($n = 18$ cells).

Data are mean \pm SEM and were analyzed by paired (B–D), unpaired (E–G and J) t test, and linear regression (H and K, Pearson's correlation). ** $p < 0.01$, *** $p < 0.001$. Scale bar: 3 μ m (I). See also Figures S3 and S4 and Table S3.

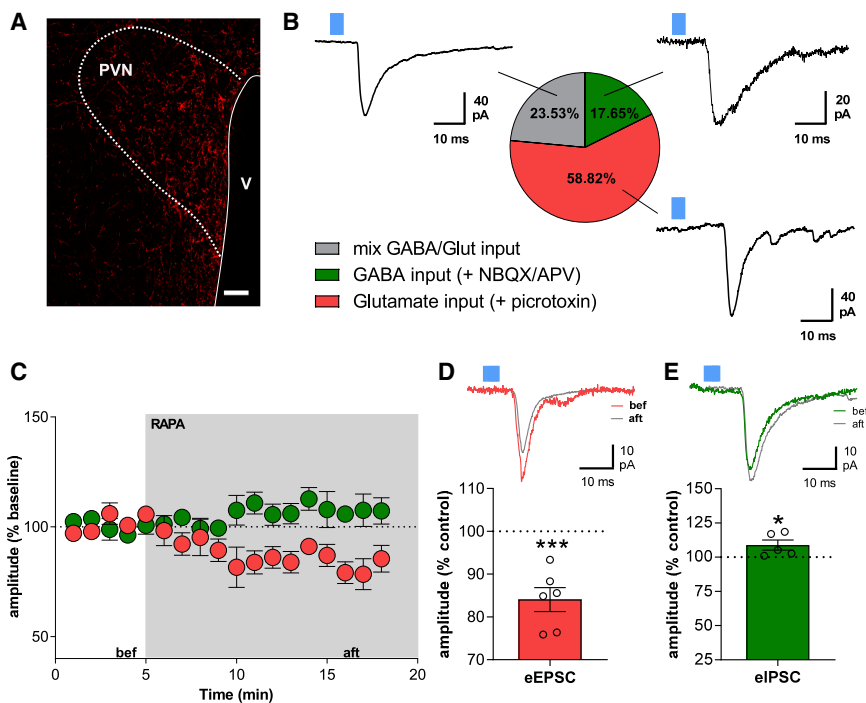


Figure 5. mTORC1 activity modulates POMC neuron neurotransmission onto PVN parvocellular cells

(A) Representative image of mCherry-positive, Chr2-expressing projections from ARC POMC neurons onto the hypothalamic PVN.

(B) Distribution of the neurotransmission type recorded in PVN parvocellular neurons after photostimulation ($n = 17$ cells) and representative traces of light-evoked post-synaptic currents for each neurotransmission type. POMC neurons mainly release glutamate (58.82%, 10/17 cells) onto parvocellular neurons; pure GABAergic (17.65%; 3/17 cells) and mixed GABA/glutamate (23.53%, 4/17 cells) connections were also found.

(C) Amplitude time course of light-evoked EPSCs (red; $n = 6$ cells) and IPSCs (green; $n = 5$ cells) normalized to baseline.

(D and E) RAPA decreases eEPSCs amplitude (**D**) and increases eIPSCs amplitude (**E**). Representative traces of eEPSC (**D**; top) and eIPSC (**E**; top) before (bef, in **C**) and after (aft, in **C**) RAPA application. Data are mean \pm SEM and were analyzed by paired t test (**D** and **E**). * $p < 0.05$, *** $p < 0.001$. V, 3rd ventricle. Scale bar: 50 μ m (**A**). Blue square: light. See also [Figure S5](#) and [Tables S2](#) and [S3](#).

expression of markers of fuel substrates use and synaptic activity. POMC/GABAergic neurons were enriched in the expression of genes that regulate glucose and lipid metabolism, protein transcription and catabolism ([Table 1](#)), whereas POMC/glutamatergic neurons had increased expression of genes involved in synaptic vesicular function, purine metabolism, and GTP signaling ([Table 1](#)). These different POMC neurons subpopulations also had specific spatial distribution, as assessed by analyzing their rostro-caudal distribution and the distance from the third ventricle by FISH ([Figures 6B–6D](#), [S7B](#), and [S7C](#)). POMC/glutamatergic neurons were generally farthest from the ventricle and had a rostro-caudal decrease, while POMC/GABAergic neurons were closest to the ventricle and had a rostro-caudal increase. Mixed GABA/glutamatergic cells and POMC cells negative for the two neurotransmitters were somewhat in between ([Figures 6B–6D](#) and [S7B](#)). Hence different hypothalamic POMC/neurotransmitter-type subpopulations have specific molecular signatures and spatial distribution.

DISCUSSION

Over the past 20 years, several studies have outlined the functions of POMC and AgRP neurons in the context of energy balance regulation, leading to the widespread notion that POMC neurons decrease food intake, whereas AgRP neurons increase it. If POMC neurons decode only a satiety signal, as postulated by the prevailing view in the field, one should expect that their activation immediately stops food consumption. However, fiber photometry studies have shown that AgRP neurons are switched off and POMC neurons become active as soon as animals start eating ([Brandt et al., 2018](#); [Chen et al., 2015](#)). This emerging evidence argues against an exclusive role of POMC neurons in eating cessation. Given

the high degree of molecular heterogeneity and functional plasticity of these cells, multiple POMC neuronal subtypes may have a divergent impact on feeding behavior ([Biglari et al., 2021](#); [Quarta et al., 2021](#)). However, the exact identity of the main molecular signals that link such functional plasticity with feeding responses is far from being understood.

We now show that POMC neuron functional heterogeneity relies on mTORC1 signaling. After a prolonged fast, POMC neuronal subpopulations that respond to changes in mTORC1 signaling may initially favor ingestion of food via concomitant activation of GABAergic transmission and inhibition of glutamatergic action. Once energy levels have risen, concomitant increases in melanocortin and POMC/glutamatergic signaling and inhibition of POMC/GABAergic activity would then help terminate the meal. This interpretation is supported by our observation that POMC/GABAergic cells activated by RAPA, which mimics a negative energy state, have similar electrophysiological characteristics as those cells that are inhibited by leptin, which mimics a positive energy state. Vice versa, those POMC neurons that are inhibited by RAPA and that display a glutamatergic phenotype have similar electrophysiological properties as those POMC cells that are activated by leptin.

Besides, our optogenetic experiments reveal that mTORC1 activity simultaneously and oppositely modulates the activity of POMC/GABAergic and POMC/glutamatergic neurons, which, together with the additional evidence we provide, suggest an opposite action of these POMC cells subtypes on food intake. Our single-cell RNA-seq analysis also revealed that POMC/GABAergic and POMC/glutamatergic subpopulations are molecularly distinct, but both express components of the mTOR pathway in a similar fashion. Hence the divergent cellular

Table 1. Gene annotation enrichment analysis of differentially expressed genes in POMC/GABAergic and POMC/glutamatergic neurons

Database	Term	Fold enrichment	Count	p value
Enriched in POMC/GABA neurons				
Gene Ontology	glutamate decarboxylase activity	67.11	2	2.94E−2
Gene Ontology	glucose-6-phosphate/hexose phosphate transport	45.07	2	4.35E−2
Gene Ontology	transcriptional repressor complex	11.75	5	7.79E−4
Gene Ontology	proteasomal ubiquitin-dependent protein catabolic process	9.01	4	9.52E−3
Gene Ontology	neutral lipid metabolic process	6.01	4	2.84E−2
Gene Ontology	glycerol ether metabolic process	6.01	4	2.84E−2
Gene Ontology	triglyceride metabolic process	5.63	3	9.81E−2
Gene Ontology	chromatin binding	4.33	10	5.03E−4
Gene Ontology	regulation of gene-specific transcription	4.04	4	7.59E−2
Gene Ontology	transcription coactivator activity	4.03	6	1.65E−2
Gene Ontology	transcription cofactor activity	3.82	12	3.10E−4
Gene Ontology	transcription repressor activity	3.73	10	1.45E−3
Gene Ontology	transcription corepressor activity	3.73	4	9.12E−2
Gene Ontology	glycerolipid metabolic process	3.14	6	4.19E−2
Gene Ontology	ubiquitin-dependent protein catabolic process	2.88	6	5.74E−2
Gene Ontology	transcription factor binding	2.80	12	3.82E−3
Gene Ontology	negative regulation of transcription	2.54	14	3.56E−3
Gene Ontology	negative regulation of gene expression	2.47	15	3.04E−3
Gene Ontology	transcription factor complex	2.25	8	6.50E−2
Enriched in POMC/Glut neurons				
Gene Ontology	synaptic vesicle membrane	34.64	2	5.48E−2
Gene Ontology	synaptic vesicle membrane	34.64	2	5.48E−2
Gene Ontology	clathrin-coated vesicle membrane	27.42	3	5.04E−3
Gene Ontology	cytoplasmic vesicle membrane	11.35	3	2.72E−2
KEGG pathway	purine metabolism	7.31	3	5.46E−02
Gene Ontology	GTP binding	4.42	4	5.68E−2
Gene Ontology	vesicle	3.17	5	6.59E−2

in hypothalamic levels of the appetite-suppressant α -MSH and the appetite-stimulant AEA, which eventually modulated the feeding response and neurotransmitter release. Although future investigations will need to determine the molecular mechanisms underlying the changes of these appetite-related signals in response to mTORC1 modulation, our data showed that endocannabinoid-dependent activation of CB₁R downstream of POMC neurons has a role in determining RAPA-induced hyperphagia. However, CB₁R activation in POMC neurons restrained food intake by likely blunting POMC/GABAergic transmission, as suggested by the combined administration of RAPA with the GABA_A antagonist Ptx in POMC-CB₁-KO mice. These findings agree with past work demonstrating that activation of CB₁R signaling in GABAergic neurons decreases food intake (Bellocchio et al., 2010; Soria-Gómez et al., 2014a).

As already mentioned, transcriptomic profiling in the hypothalamus of C57BL/6 mice revealed that POMC/glutamatergic and

POMC/GABAergic subpopulations have distinct neurochemical features. Importantly, we also found that a small fraction of POMC/GABAergic neurons co-express *Npy* and/or *Agrp*, implying that there is a subgroup of hypothalamic GABAergic cells that contains both POMC and AgRP in adulthood. This agrees with previous transcriptomic data obtained using reporter mice to trace POMC and AgRP neurons (Lam et al., 2017) and likely reflects the shared developmental origins of POMC and NPY/AgRP cells (Padilla et al., 2010), indicating that these features are present in C57BL/6 mice and are conserved during adult life. This evidence also highlights the intrinsic limitation of any study, including ours, using genetic models generated with a POMC-Cre transgene induced during either development or adulthood, because these approaches may leave out the possibility that some of the effects observed involve POMC cells expressing also NPY/AgRP.

As for the specific roles of POMC/GABAergic or glutamatergic neurons subpopulations in the context of food intake or energy

balance, recent studies have shown that re-expression of POMC in either GABAergic or glutamatergic neurons of obese mice with conditionally silenced *Pomc* alleles decreases food intake and body weight, correcting the obese phenotype (Jones et al., 2019; Trotta et al., 2020), although genetic removal of either the glutamatergic or GABAergic component seem not sufficient to affect food intake (Rau et al., 2020). These genetic models, however, also target POMC mixed GABA/glutamatergic cells. Thus, it will be particularly relevant to develop new animal models that will allow dissecting the specific and redundant roles played by different POMC neurons subpopulations, including those neuronal clusters with a mixed GABA/glutamatergic phenotype. The recent use of intersectional targeting to manipulate the activity of molecularly distinct POMC neuronal subtypes (Biglari et al., 2021) could be applied to address some of the relevant questions that arise from our work. Our neuroanatomical studies further support the idea that POMC/glutamatergic and POMC/GABAergic subtypes may have distinct physiological roles, given their specific spatial location in the ARC. Such a distinct spatial distribution could be associated with a specific projections profile, because it has been shown for AgRP neurons (Betley et al., 2013). Noteworthy, the heterogeneity in neurotransmitter type might explain the observation that activation of POMC neurons by opto- or chemo-genetics does not translate into acute, rapid (within hours) changes in food intake (present findings and Aponte et al., 2011; Koch et al., 2015; Zhan et al., 2013). Likewise, our observation that POMC-*Rptor*-KO, POMC-*Rictor*-KO, and POMC-*CB₁*-KO mice did not have a phenotype during acute refeeding could be because of the expression of the deleted genes across the different POMC neuronal subpopulations and the counterbalancing physiological functions of these functionally divergent subpopulations. Alternatively, the lack of phenotype could be because of developmental compensation. This remains a possibility, albeit specific effects on food intake and electrophysiological responses were observed in these models (present findings and Haissaguerre et al., 2018; Mazier et al., 2019).

In conclusion, the present study provides compelling evidence for a more sophisticated role of POMC neurons in the regulation of acute feeding responses than what we have so far believed. Indeed, specific subpopulations of these neurons may differentially impact this behavior in response to changes in mTORC1 activity. These findings reveal an unforeseen neuronal mechanism, which modifies our notion of hypothalamic circuits regulating food intake, energy balance, and possibly their associated pathological states.

STAR★METHODS

Detailed methods are provided in the online version of this paper and include the following:

- KEY RESOURCES TABLE
- RESOURCE AVAILABILITY
 - Lead contact
 - Materials availability
 - Data and code availability
- EXPERIMENTAL MODEL AND SUBJECT DETAILS
 - Mice

● METHOD DETAILS

- PCR for mouse genotyping
- AAV vectors for hM3Dq and channelrhodopsin-2 (ChR2) expression
- Stereotaxic surgery
- Stereotaxic virus injection
- Food intake studies
- Immunohistochemistry (IHC)
- Fluorescent *in situ* hybridization (FISH)
- Electrophysiology

● QUANTIFICATION AND STATISTICAL ANALYSIS

SUPPLEMENTAL INFORMATION

Supplemental information can be found online at <https://doi.org/10.1016/j.celrep.2021.109800>.

ACKNOWLEDGMENTS

We thank the animal, genotyping, and bioinformatics platforms of the INSERM U1215, funded by INSERM and Labex Brain, for animal care, management of mouse lines, and genotyping. We thank the analytical chemistry facility of the INSERM U1215, funded by INSERM, for quantification of endocannabinoids and UT Southwestern and IGBMC for POMC-CreERT2 mice. The microscopy was done in the Bordeaux Imaging Center, a service unit of the CNRS-INSERM and Bordeaux University, member of the national infrastructure France Bio-Imaging supported by the Labex Brain. The help of F. Cordelières, C. Poujol, S. Marais, and P. Mascalchi (University of Bordeaux) is acknowledged. We thank the biochemistry and biophysics platform of Bordeaux NeuroCampus, supported by the Labex Brain; Dr. A. Zeisel and Dr. S. Linnarsson (Karolinska Institutet, Stockholm, Sweden) for help with single-cell RNA-seq studies; and K. Parker (Harvard University) for designing the probes of the triple FISH study. We thank Drs. S.C. Woods (University of Cincinnati), F. Chaouloff, and P. Ciofi (INSERM U1215) for useful suggestions. This work was supported by INSERM (D.C., C.Q., and G.M.), Aquitaine Region, ANR [ANR-13-BSV4-0006, ANR-18-CE14-0029 MitObesity, and Labex BRAIN ANR-10-LABX-43 (D.C., G.M.); ANR-2010-1414-01, ANR-10-EQX-008-1 OPTOPATH, ANR-17-CE14-0007 BABrain (D.C.); ANR-16-CE37-0010 (G.M.); and ANR-20-CE14-0046 (C.Q.)]; FFRD (D.C.); INSERM/Aquitaine Region PhD fellowship and FRM PhD fellowship FDT20150532545 (N.S.); PhD fellowship from the French Ministry for Higher Education, Research and Innovation and FRM PhD fellowship FDT201805005371 (V.S.); PhD fellowship from the French Ministry for Higher Education, Research and Innovation (S.L.); French Societies of Endocrinology (SFE), Nutrition (SFN), and Diabetes (SFD) (C.Q.); European Commission [Marie Curie IRG n°224757 (D.C.), HEALTH-F2-2008-223713 and HEALTH-603191 (G.M.), FP7-People2009-IEF-251494 (D.C., E.B.), ERC-2010-StG-260515 and ERC-2014-PoC-640923 (G.M.)], and FRM (C.C., F.M., L.B., G.M.); Postgraduate Scholarship Programme of the Free State of Saxony and Erasmus Traineeship Programme (J.M.B.); a New York Stem Cell Foundation – Robertson Investigator (F.T.M.) supported by the Medical Research Council (MR/P501967/1) and the Wellcome Trust and Royal Society (211221/Z/18/Z); NIH DK080003 (S.L.W.); Swedish Research Council, Hjärfonden, the Novo Nordisk Foundation, ERC SECRET-CELLS, intramural funds of the Medical University of Vienna (T.H.); and EMBO long-term research fellowship ALTF 596-2014 and Marie Curie Actions EMBO-COFUND2012 GA-2012-600394 (R.A.R.).

AUTHOR CONTRIBUTIONS

N.S., W.M., V.S., E.B., C.C., L.B., R.A.R., I.M., P.Z., S.L., C.Q., A.C., K.M., D.G., S.C., and J.M.B. generated the data; N.S., W.M., V.S., G.S.H.Y., X.F., F.T.M., S.L.W., T.H., F.M., and D.C. analyzed the data together with the other authors; X.F., T.H., F.M., and G.M. critically contributed to discussion; D.C. conceptualized all studies and supervised the work; N.S., W.M., V.S., and D.C. wrote the manuscript; all authors edited and approved the final version of the manuscript.

DECLARATION OF INTERESTS

The authors declare no competing interests.

Received: November 13, 2020

Revised: July 21, 2021

Accepted: September 15, 2021

Published: October 12, 2021

REFERENCES

- Alexander, G.M., Rogan, S.C., Abbas, A.I., Armbruster, B.N., Pei, Y., Allen, J.A., Nonneman, R.J., Hartmann, J., Moy, S.S., Nicolelis, M.A., et al. (2009). Remote control of neuronal activity in transgenic mice expressing evolved G protein-coupled receptors. *Neuron* 63, 27–39.
- Aponte, Y., Atasoy, D., and Sternson, S.M. (2011). AGRP neurons are sufficient to orchestrate feeding behavior rapidly and without training. *Nat. Neurosci.* 14, 351–355.
- Atasoy, D., Aponte, Y., Su, H.H., and Sternson, S.M. (2008). A FLEX switch targets Channelrhodopsin-2 to multiple cell types for imaging and long-range circuit mapping. *J. Neurosci.* 28, 7025–7030.
- Balthasar, N., Coppari, R., McMinn, J., Liu, S.M., Lee, C.E., Tang, V., Kenny, C.D., McGovern, R.A., Chua, S.C., Jr., Elmquist, J.K., and Lowell, B.B. (2004). Leptin receptor signaling in POMC neurons is required for normal body weight homeostasis. *Neuron* 42, 983–991.
- Balthasar, N., Dalgaard, L.T., Lee, C.E., Yu, J., Funahashi, H., Williams, T., Ferreira, M., Tang, V., McGovern, R.A., Kenny, C.D., et al. (2005). Divergence of melanocortin pathways in the control of food intake and energy expenditure. *Cell* 123, 493–505.
- Bellocchio, L., Lafenêtre, P., Cannich, A., Cota, D., Puente, N., Grandes, P., Chaouloff, F., Piazza, P.V., and Marsicano, G. (2010). Bimodal control of stimulated food intake by the endocannabinoid system. *Nat. Neurosci.* 13, 281–283.
- Bellocchio, L., Soría-Gómez, E., Quarta, C., Metna-Laurent, M., Cardinal, P., Binder, E., Cannich, A., Delamarre, A., Häring, M., Martín-Fontecha, M., et al. (2013). Activation of the sympathetic nervous system mediates hypophagic and anxiety-like effects of CB₁ receptor blockade. *Proc. Natl. Acad. Sci. USA* 110, 4786–4791.
- Berglund, E.D., Liu, C., Sohn, J.W., Liu, T., Kim, M.H., Lee, C.E., Vianna, C.R., Williams, K.W., Xu, Y., and Elmquist, J.K. (2013). Serotonin 2C receptors in pro-opiomelanocortin neurons regulate energy and glucose homeostasis. *J. Clin. Invest.* 123, 5061–5070.
- Betley, J.N., Cao, Z.F., Ritola, K.D., and Sternson, S.M. (2013). Parallel, redundant circuit organization for homeostatic control of feeding behavior. *Cell* 155, 1337–1350.
- Biglari, N., Gaziano, I., Schumacher, J., Radermacher, J., Paeger, L., Klemm, P., Chen, W., Corneliussen, S., Wunderlich, C.M., Sue, M., et al. (2021). Functionally distinct POMC-expressing neuron subpopulations in hypothalamus revealed by intersectional targeting. *Nat. Neurosci.* 24, 913–929.
- Bockaert, J., and Marin, P. (2015). mTOR in Brain Physiology and Pathologies. *Physiol. Rev.* 95, 1157–1187.
- Brandt, C., Nolte, H., Henschke, S., Engström Ruud, L., Awazawa, M., Morgan, D.A., Gabel, P., Sprenger, H.G., Hess, M.E., Günther, S., et al. (2018). Food Perception Primes Hepatic ER Homeostasis via Melanocortin-Dependent Control of mTOR Activation. *Cell* 175, 1321–1335.e20.
- Brown, L.M., Clegg, D.J., Benoit, S.C., and Woods, S.C. (2006). Intraventricular insulin and leptin reduce food intake and body weight in C57BL/6J mice. *Physiol. Behav.* 89, 687–691.
- Burke, L.K., Darwish, T., Cavanaugh, A.R., Virtue, S., Roth, E., Morro, J., Liu, S.M., Xia, J., Dalley, J.W., Burling, K., et al. (2017). mTORC1 in AGRP neurons integrates exteroceptive and interoceptive food-related cues in the modulation of adaptive energy expenditure in mice. *eLife* 6, e22848.
- Busquets-García, A., Bains, J., and Marsicano, G. (2018). CB₁ Receptor Signaling in the Brain: Extracting Specificity from Ubiquity. *Neuropsychopharmacology* 43, 4–20.
- Campbell, J.N., Macosko, E.Z., Fenselau, H., Pers, T.H., Lyubetskaya, A., Tenen, D., Goldman, M., Verstegen, A.M., Resch, J.M., McCarroll, S.A., et al. (2017). A molecular census of arcuate hypothalamus and median eminence cell types. *Nat. Neurosci.* 20, 484–496.
- Chen, Y., Lin, Y.C., Kuo, T.W., and Knight, Z.A. (2015). Sensory detection of food rapidly modulates arcuate feeding circuits. *Cell* 160, 829–841.
- Cota, D., Proulx, K., Smith, K.A., Kozma, S.C., Thomas, G., Woods, S.C., and Seeley, R.J. (2006). Hypothalamic mTOR signaling regulates food intake. *Science* 312, 927–930.
- Cota, D., Proulx, K., and Seeley, R.J. (2007). The role of CNS fuel sensing in energy and glucose regulation. *Gastroenterology* 132, 2158–2168.
- Courtin, J., Chaudun, F., Rozeske, R.R., Karalis, N., Gonzalez-Campo, C., Wurtz, H., Abdi, A., Baufreton, J., Bienvenu, T.C., and Herry, C. (2014). Prefrontal parvalbumin interneurons shape neuronal activity to drive fear expression. *Nature* 505, 92–96.
- Dagon, Y., Hur, E., Zheng, B., Wellenstein, K., Cantley, L.C., and Kahn, B.B. (2012). p70S6 kinase phosphorylates AMPK on serine 491 to mediate leptin's effect on food intake. *Cell Metab.* 16, 104–112.
- Dennis, G., Jr., Sherman, B.T., Hosack, D.A., Yang, J., Gao, W., Lane, H.C., and Lempicki, R.A. (2003). DAVID: Database for Annotation, Visualization, and Integrated Discovery. *Genome Biol.* 4, 3.
- Dicken, M.S., Tooker, R.E., and Hentges, S.T. (2012). Regulation of GABA and glutamate release from proopiomelanocortin neuron terminals in intact hypothalamic networks. *J. Neurosci.* 32, 4042–4048.
- Dietrich, M.O., and Horvath, T.L. (2013). Hypothalamic control of energy balance: insights into the role of synaptic plasticity. *Trends Neurosci.* 36, 65–73.
- Fekete, C., Zséli, G., Singru, P.S., Kádár, A., Wittmann, G., Füzesi, T., El-Bermani, W., and Lechan, R.M. (2012). Activation of anorexigenic pro-opiomelanocortin neurons during refeeding is independent of vagal and brainstem inputs. *J. Neuroendocrinol.* 24, 1423–1431.
- Fenselau, H., Campbell, J.N., Verstegen, A.M., Madara, J.C., Xu, J., Shah, B.P., Resch, J.M., Yang, Z., Mandelblat-Cerf, Y., Livneh, Y., and Lowell, B.B. (2017). A rapidly acting glutamatergic ARC→PVH satiety circuit postsynaptically regulated by α -MSH. *Nat. Neurosci.* 20, 42–51.
- Gatta-Cherifi, B., Matias, I., Vallée, M., Tabarin, A., Marsicano, G., Piazza, P.V., and Cota, D. (2012). Simultaneous postprandial deregulation of the orexigenic endocannabinoid anandamide and the anorexigenic peptide YY in obesity. *Int. J. Obes.* 36, 880–885.
- Gomez, J.L., Bonaventura, J., Lesniak, W., Mathews, W.B., Sysa-Shah, P., Rodriguez, L.A., Ellis, R.J., Richie, C.T., Harvey, B.K., Dannals, R.F., et al. (2017). Chemogenetics revealed: DREADD occupancy and activation via converted clozapine. *Science* 357, 503–507.
- Haissaguerre, M., Saucisse, N., and Cota, D. (2014). Influence of mTOR in energy and metabolic homeostasis. *Mol. Cell. Endocrinol.* 397, 67–77.
- Haissaguerre, M., Ferrière, A., Simon, V., Saucisse, N., Dupuy, N., André, C., Clark, S., Guzman-Quevedo, O., Tabarin, A., and Cota, D. (2018). mTORC1-dependent increase in oxidative metabolism in POMC neurons regulates food intake and action of leptin. *Mol. Metab.* 12, 98–106.
- Hara, K., Maruki, Y., Long, X., Yoshino, K., Oshiro, N., Hidayat, S., Tokunaga, C., Avruch, J., and Yonezawa, K. (2002). Raptor, a binding partner of target of rapamycin (TOR), mediates TOR action. *Cell* 110, 177–189.
- Henry, F.E., Sugino, K., Tozer, A., Branco, T., and Sternson, S.M. (2015). Cell type-specific transcriptomics of hypothalamic energy-sensing neuron responses to weight-loss. *eLife* 4, e09800.
- Hentges, S.T., Nishiyama, M., Overstreet, L.S., Stenzel-Poore, M., Williams, J.T., and Low, M.J. (2004). GABA release from proopiomelanocortin neurons. *J. Neurosci.* 24, 1578–1583.
- Hentges, S.T., Otero-Corchon, V., Pennock, R.L., King, C.M., and Low, M.J. (2009). Proopiomelanocortin expression in both GABA and glutamate neurons. *J. Neurosci.* 29, 13684–13690.
- Huang, D.W., Sherman, B.T., and Lempicki, R.A. (2009). Systematic and integrative analysis of large gene lists using DAVID bioinformatics resources. *Nat. Protoc.* 4, 44–57.

- Jones, G.L., Wittmann, G., Yokosawa, E.B., Yu, H., Mercer, A.J., Lechan, R.M., and Low, M.J. (2019). Selective Restoration of *Pomc* Expression in Glutamatergic POMC Neurons: Evidence for a Dynamic Hypothalamic Neurotransmitter Network. *eNeuro* 6, ENEURO.0400-18.2019.
- Kirkham, T.C., Williams, C.M., Fezza, F., and Di Marzo, V. (2002). Endocannabinoid levels in rat limbic forebrain and hypothalamus in relation to fasting, feeding and satiation: stimulation of eating by 2-arachidonoyl glycerol. *Br. J. Pharmacol.* 136, 550–557.
- Koch, M., Varela, L., Kim, J.G., Kim, J.D., Hernández-Nuño, F., Simonds, S.E., Castorena, C.M., Vianna, C.R., Elmquist, J.K., Morozov, Y.M., et al. (2015). Hypothalamic POMC neurons promote cannabinoid-induced feeding. *Nature* 519, 45–50.
- Kozorovitskiy, Y., Saunders, A., Johnson, C.A., Lowell, B.B., and Sabatini, B.L. (2012). Recurrent network activity drives striatal synaptogenesis. *Nature* 485, 646–650.
- Krashes, M.J., Lowell, B.B., and Garfield, A.S. (2016). Melanocortin-4 receptor-regulated energy homeostasis. *Nat. Neurosci.* 19, 206–219.
- Lam, B.Y.H., Cimino, I., Poxel-Wolf, J., Nicole Kohnke, S., Rimmington, D., Iyemere, V., Heeley, N., Cossetti, C., Schulte, R., Saraiva, L.R., et al. (2017). Heterogeneity of hypothalamic pro-opiomelanocortin-expressing neurons revealed by single-cell RNA sequencing. *Mol. Metab.* 6, 383–392.
- Luther, J.A., and Tasker, J.G. (2000). Voltage-gated currents distinguish parvocellular from magnocellular neurones in the rat hypothalamic paraventricular nucleus. *J. Physiol.* 523, 193–209.
- Marsicano, G., Wotjak, C.T., Azad, S.C., Bisogno, T., Rammes, G., Cascio, M.G., Hermann, H., Tang, J., Hofmann, C., Ziegler, W., et al. (2002). The endogenous cannabinoid system controls extinction of aversive memories. *Nature* 418, 530–534.
- Marsicano, G., Goodenough, S., Monory, K., Hermann, H., Eder, M., Cannich, A., Azad, S.C., Cascio, M.G., Gutiérrez, S.O., van der Stelt, M., et al. (2003). CB1 cannabinoid receptors and on-demand defense against excitotoxicity. *Science* 302, 84–88.
- Mazier, W., Saucisse, N., Gatta-Cherifi, B., and Cota, D. (2015). The Endocannabinoid System: Pivotal Orchestrator of Obesity and Metabolic Disease. *Trends Endocrinol. Metab.* 26, 524–537.
- Mazier, W., Saucisse, N., Simon, V., Cannich, A., Marsicano, G., Massa, F., and Cota, D. (2019). mTORC1 and CB1 receptor signaling regulate excitatory glutamatergic inputs onto the hypothalamic paraventricular nucleus in response to energy availability. *Mol. Metab.* 28, 151–159.
- Monge-Roffarello, B., Labbe, S.M., Roy, M.C., Lemay, M.L., Coneggo, E., Samson, P., Lanfray, D., and Richard, D. (2014). The PVH as a site of CB1-mediated stimulation of thermogenesis by MC4R agonism in male rats. *Endocrinology* 155, 3448–3458.
- Monory, K., Massa, F., Egertová, M., Eder, M., Blaudzun, H., Westenbroek, R., Kelsch, W., Jacob, W., Marsch, R., Ekker, M., et al. (2006). The endocannabinoid system controls key epileptogenic circuits in the hippocampus. *Neuron* 51, 455–466.
- Padilla, S.L., Carmody, J.S., and Zeltser, L.M. (2010). *Pomc*-expressing progenitors give rise to antagonistic neuronal populations in hypothalamic feeding circuits. *Nat. Med.* 16, 403–405.
- Papadopoulos, A.D., and Wardlaw, S.L. (1999). Endogenous alpha-MSH modulates the hypothalamic-pituitary-adrenal response to the cytokine interleukin-1beta. *J. Neuroendocrinol.* 11, 315–319.
- Quarta, C., Claret, M., Zeltser, L.M., Williams, K.W., Yeo, G.S.H., Tschöp, M.H., Diano, S., Brüning, J.C., and Cota, D. (2021). POMC neuronal heterogeneity in energy balance and beyond: an integrated view. *Nat. Metab.* 3, 299–308.
- R Core Team (2020). R: A language and environment for statistical computing (R Foundation for Statistical Computing).
- Rau, A.R., King, C.M., and Hentges, S.T. (2020). Disruption of GABA or glutamate release from POMC neurons in the adult mouse does not affect metabolic end points. *Am. J. Physiol. Regul. Integr. Comp. Physiol.* 319, R592–R601.
- Reich, M., Liefeld, T., Gould, J., Lerner, J., Tamayo, P., and Mesirov, J.P. (2006). GenePattern 2.0. *Nat. Genet.* 38, 500–501.
- Romanov, R.A., Zeisel, A., Bakker, J., Girach, F., Hellyasz, A., Tomer, R., Alpár, A., Mulder, J., Clotman, F., Keimpema, E., et al. (2017). Molecular interrogation of hypothalamic organization reveals distinct dopamine neuronal subtypes. *Nat. Neurosci.* 20, 176–188.
- Sarbasov, D.D., Ali, S.M., Kim, D.H., Guertin, D.A., Latek, R.R., Erdjument-Bromage, H., Tempst, P., and Sabatini, D.M. (2004). Rictor, a novel binding partner of mTOR, defines a rapamycin-insensitive and raptor-independent pathway that regulates the cytoskeleton. *Curr. Biol.* 14, 1296–1302.
- Savontaus, E., Breen, T.L., Kim, A., Yang, L.M., Chua, S.C., Jr., and Wardlaw, S.L. (2004). Metabolic effects of transgenic melanocyte-stimulating hormone overexpression in lean and obese mice. *Endocrinology* 145, 3881–3891.
- Schneider, C.A., Rasband, W.S., and Eliceiri, K.W. (2012). NIH Image to ImageJ: 25 years of image analysis. *Nat. Methods* 9, 671–675.
- Singru, P.S., Sánchez, E., Fekete, C., and Lechan, R.M. (2007). Importance of melanocortin signaling in refeeding-induced neuronal activation and satiety. *Endocrinology* 148, 638–646.
- Singru, P.S., Wittmann, G., Farkas, E., Zséli, G., Fekete, C., and Lechan, R.M. (2012). Refeeding-activated glutamatergic neurons in the hypothalamic paraventricular nucleus (PVN) mediate effects of melanocortin signaling in the nucleus tractus solitarius (NTS). *Endocrinology* 153, 3804–3814.
- Smith, M.A., Katsouri, L., Irvine, E.E., Hankir, M.K., Pedroni, S.M., Voshol, P.J., Gordon, M.W., Choudhury, A.I., Woods, A., Vidal-Puig, A., et al. (2015). Ribosomal S6K1 in POMC and AgRP Neurons Regulates Glucose Homeostasis but Not Feeding Behavior in Mice. *Cell Rep.* 11, 335–343.
- Soria-Gómez, E., Bellocchio, L., Reguero, L., Lepousez, G., Martin, C., Bendahmane, M., Ruehle, S., Remmers, F., Desprez, T., Matias, I., et al. (2014a). The endocannabinoid system controls food intake via olfactory processes. *Nat. Neurosci.* 17, 407–415.
- Soria-Gómez, E., Massa, F., Bellocchio, L., Rueda-Orozco, P.E., Ciofi, P., Cota, D., Oliet, S.H., Prospéro-García, O., and Marsicano, G. (2014b). Cannabinoid type-1 receptors in the paraventricular nucleus of the hypothalamus inhibit stimulated food intake. *Neuroscience* 263, 46–53.
- Tong, Q., Ye, C.P., Jones, J.E., Elmquist, J.K., and Lowell, B.B. (2008). Synaptic release of GABA by AgRP neurons is required for normal regulation of energy balance. *Nat. Neurosci.* 11, 998–1000.
- Trotta, M., Bello, E.P., Alsina, R., Tavella, M.B., Ferrán, J.L., Rubinstein, M., and Bumashny, V.F. (2020). Hypothalamic *Pomc* expression restricted to GABAergic neurons suppresses *Npy* overexpression and restores food intake in obese mice. *Mol. Metab.* 37, 100985.
- Tsigos, C., Crosby, S.R., Gibson, S., Young, R.J., and White, A. (1993). Pro-opiomelanocortin is the predominant adrenocorticotropic-related peptide in human cerebrospinal fluid. *J. Clin. Endocrinol. Metab.* 76, 620–624.
- Verty, A.N., McFarlane, J.R., McGregor, I.S., and Mallet, P.E. (2004). Evidence for an interaction between CB1 cannabinoid and melanocortin MCR-4 receptors in regulating food intake. *Endocrinology* 145, 3224–3231.
- Wardlaw, S.L. (2011). Hypothalamic proopioidmelanocortin processing and the regulation of energy balance. *Eur. J. Pharmacol.* 660, 213–219.
- Weston, M.C., Chen, H., and Swann, J.W. (2012). Multiple roles for mammalian target of rapamycin signaling in both glutamatergic and GABAergic synaptic transmission. *J. Neurosci.* 32, 11441–11452.
- Wittmann, G., Hrabovszky, E., and Lechan, R.M. (2013). Distinct glutamatergic and GABAergic subsets of hypothalamic pro-opiomelanocortin neurons revealed by in situ hybridization in male rats and mice. *J. Comp. Neurol.* 521, 3287–3302.
- Zhan, C., Zhou, J., Feng, Q., Zhang, J.E., Lin, S., Bao, J., Wu, P., and Luo, M. (2013). Acute and long-term suppression of feeding behavior by POMC neurons in the brainstem and hypothalamus, respectively. *J. Neurosci.* 33, 3624–3632.

STAR★METHODS

KEY RESOURCES TABLE

REAGENT or RESOURCE	SOURCE	IDENTIFIER
Antibodies		
Goat polyclonal anti-c-Fos	Santa Cruz Biotechnology	Cat#sc-52-G; RRID: AB_2629503
Rabbit polyclonal anti-GAD65/67	Millipore	Cat# AB1511; RRID: AB_90715
Rabbit polyclonal anti-POMC	Phoenix Pharmaceuticals	Cat#H-029-30; RRID: AB_2307442
Rabbit polyclonal anti-p-S6 ser240/244	Cell Signaling Technology	Cat#2215; RRID: AB_331682
Rabbit polyclonal anti-Rictor	Bethyl Laboratories, Inc.	Cat#A300-459A; RRID: AB_2179967
Donkey anti-goat IgG – Alexa Fluor® 488 conjugated, IgG	Thermo Fisher Scientific	Cat#A-11055; RRID: AB_2534102
Donkey anti-goat IgG – Alexa Fluor® 594 conjugated, IgG	Thermo Fisher Scientific	Cat#A-11058; RRID: AB_2534105
Goat anti-rabbit IgG – Alexa Fluor® 488 conjugated, F(ab') ₂	Cell Signaling Technology	Cat#4412; RRID: AB_1904025
Goat anti-rabbit IgG – Alexa Fluor® 647 conjugated, F(ab') ₂	Cell Signaling Technology	Cat#4414; RRID: AB_10693544
Goat anti-rabbit IgG – AffiniPure F(ab) Fragment	Jackson ImmunoResearch Labs	Cat#111-007-003; RRID: AB_2337925
Goat anti-rabbit IgG – Biotinylated	Vector Laboratories	Cat#BA-1000; RRID: AB_2313606
Streptavidin – AMCA conjugated	Vector Laboratories	Cat#SA-5008; RRID: AB_2336103
Streptavidin – Fluorescein conjugated	Vector Laboratories	Cat#SA-5001; RRID: AB_2336462
Sheep anti-Digoxigenin – Peroxidase (POD) Conjugated, F(ab) fragments	Roche	Cat#11207733910; RRID: AB_514500
Sheep anti-Digoxigenin – Peroxidase (POD) Conjugated, F(ab) fragments	Roche	Cat#11426346910; RRID: AB_840257
Anti-DNP – Peroxidase (HRP) Conjugated	PerkinElmer	Cat#FP1129; RRID: AB_2629439
Bacterial and virus strains		
AAV1/2-DIO-hM3Dq-mCherry	This paper	Virus n° 14 lab stock
AAV1/2-DIO-hChR2-mCherry	This paper	Virus n° 36 lab stock
Chemicals, peptides, and recombinant proteins		
Acetic anhydride	Sigma-Aldrich	Cat#A6404; CAS: 108-24-7
Adenosine-5'-triphosphate (magnesium salt)	Sigma-Aldrich	Cat#A9187, CAS: 74804-12-9
4-Aminopyridine	Sigma-Aldrich	Cat#275875, CAS: 504-24-5
Aqua-Poly/Mount	Polysciences	Cat#18606
APV	Abcam	Cat#ab120003; CAS: 79055-68-8
Biocytin	Sigma-Aldrich	Cat#B4261; CAS: 576-19-2
Bovine Serum Albumin (BSA)	Sigma-Aldrich	Cat#A7030; CAS: 9048-46-8
Calcium chloride (CaCl ₂)	Sigma-Aldrich	Cat#C3306; CAS: 10035-04-8
Clozapine-N-oxide (CNO)	Sigma-Aldrich	Cat#C0832; CAS: 34233-69-7
CNQX (disodium salt)	Sigma-Aldrich	Cat#C239; CAS: 115066-14-3
D-AP5	Tocris	Cat#0106; CAS: 79055-68-8
DAPI (4',6'-diamidino-2-phenylindol)	Thermo Fisher Scientific	Cat#D1306; CAS: 28718-90-3
Diethylpyrocarbonate	Sigma-Aldrich	Cat#159220; CAS: 1609-47-8
Dimethyl sulfoxide (DMSO)	Sigma-Aldrich	Cat#D2650; CAS: 67-68-5
D-Mannitol	Sigma-Aldrich	Cat#M9647; CAS: 69-65-8
EGTA	Sigma-Aldrich	Cat#E3889; CAS: 67-42-5
Ethylene Glycol	VWR	Cat#24041.297; CAS: 107-21-1
Fluoromount-G	Electron Microscopy Sciences	Cat#17984-25
Formamide	Euromedex	Cat#1117; CAS: 75-12-7
Gabazine (SR 95531 hydrobromide)	Tocris	Cat#1262; CAS: 104104-50-9

(Continued on next page)

Continued

REAGENT or RESOURCE	SOURCE	IDENTIFIER
Glucose	Sigma-Aldrich	Cat#G5767; CAS: 50-99-7
Glycerol	Sigma-Aldrich	Cat#49781; CAS: 56-81-5
Guanosine-5'-triphosphate (sodium salt)	Sigma-Aldrich	Cat#G8877; CAS: 36051-31-7
HEPES	Sigma-Aldrich	Cat#54457; CAS: 7365-45-9
Hydrochloric acid 37% (HCl)	Sigma-Aldrich	Cat#30721; CAS: 7647-01-0
Hydrogen peroxide solution, 30% (H ₂ O ₂)	Sigma-Aldrich	Cat#H1009; CAS: 7722-84-1
Ketamine (Imalgene® 1000)	Med'Vet	GTIN: 03661103003199
Leptin (mouse, recombinant)	National Hormone and Peptide Program (NHPP)	N/A
Magnesium chloride (MgCl ₂)	Sigma-Aldrich	Cat#M2670; CAS: 7791-18-6
Magnesium sulfate (MgSO ₄)	Sigma-Aldrich	Cat#M2773; CAS: 10034-99-8
NBQX	Abcam	Cat#ab120046; CAS: 118876-58-7
Neuropeptide Y (Human, Rat, Mouse) (NPY)	Phoenix Pharmaceuticals Inc.	Cat#049-03
Normal Donkey Serum (NDS)	Jackson ImmunoResearch Labs	Cat# 017-000-121, RRID:AB_2337258
Normal Goat Serum (NGS)	Agilent Technologies	Cat#X0907
OCT embedding medium	Thermo Fisher Scientific	Cat#12678646
Paraformaldehyde (PFA), prilled	Sigma-Aldrich	Cat#441244; CAS: 30525-89-4
Pentobarbital® Sodique	Ceva Santé Animale	CAS: 57-33-0
Picric Acid	Sigma-Aldrich	Cat#197378; CAS: 88-89-1
Picrotoxin (Ptx)	Sigma-Aldrich	Cat#P1675; CAS: 124-87-8
Phosphocreatine	Sigma-Aldrich	Cat#P7936; CAS: 19333-65-4
Potassium chloride (KCl)	Supelco	Cat#1.04936; CAS: 7447-40-7
Potassium gluconate	Sigma-Aldrich	Cat#G4500; CAS: 299-27-4
Potassium hydroxide (KOH)	Fluka Analytical	Cat#35113; CAS: 1310-58-3
ProLong Gold Antifade Mountant	Thermo Fisher Scientific	Cat#P36930
Rapamycin (RAPA)	Sigma-Aldrich	Cat#553210; CAS: 53123-88-9
Rimonabant (SR 141716)	NIMH Chemical Synthesis and Drug Supply Program	Cat#S-705; CAS: 168273-06-1
Saline (NaCl 0.9%)	COOPER	N/A
Saline Sodium Citrate (SSC)	Eurobio Scientific	Cat#GHYSSC00-08
Sodium bicarbonate (NaHCO ₃)	Sigma-Aldrich	Cat#S5761; CAS: 144-55-8
Sodium chloride (NaCl)	Sigma-Aldrich	Cat#S3014; CAS: 7647-14-5
Sodium dihydrogen phosphate (NaH ₂ PO ₄)	SAFC	Cat#1.06345; CAS: 13472-35-0
Sucrose	Euromedex	Cat#200-301-B; CAS: 57-50-1
Tamoxifen	Sigma-Aldrich	Cat#T5648; CAS: 10540-29-1
Tetrodotoxin (TTX)	Toocris	Cat#1069; CAS: 18660-81-6
Triethanolamine	Sigma-Aldrich	Cat#33729; CAS: 102-71-6
Triton X-100	Sigma-Aldrich	Cat#X100; CAS: 9002-93-1
TWEEN® 20	Sigma-Aldrich	Cat#P1379; CAS: 9005-64-5
WIN55-212	Sigma-Aldrich	Cat#W102; CAS: 131543-23-2
Xylazine (Rompun® 2%)	Med'Vet	GTIN: 04007221032311

Critical commercial assays

Digoxigenin-11-UTP	Roche	Cat#11209256910
DNP-11-UTP	PerkinElmer	Cat#NEL555001EA
Fluorescein-12-UTP	Roche	Cat#11427857910; CAS: 134367-01-4
MAXIsript SP6 Kit	Thermo Fisher Scientific	Cat#AM1310

(Continued on next page)

Continued

REAGENT or RESOURCE	SOURCE	IDENTIFIER
TNB Blocking Buffer	Akoya Biosciences	Cat#FP1012
TSA® Plus Cyanine 3 (Cy3)	Akoya Biosciences	Cat#NEL744001KT
TSA® Plus Cyanine 5 (Cy5)	Akoya Biosciences	Cat#NEL745001KT
TSA® Plus Fluorescein (FITC)	Akoya Biosciences	Cat#NEL741001KT
VECTASTAIN Elite ABC-Peroxidase Kit	Vector Laboratories	Cat#PK-7100; RRID: AB_2336827

Deposited data

RNA-seq data from hypothalamic neurons (C57BL/6N mice, 2-4 weeks-old)	Romanov et al., 2017	GEO: GSE74672
-----------------------------------------------------------------------	--------------------------------------	---------------

Experimental models: Organisms/strains

Mouse: C57BL/6J	Charles River	N/A
Mouse: C57BL/6J	Janvier	N/A
Mouse: <i>CB₁</i> -KO: <i>Cnr1</i> ^{tm1.1Ltz}	Marsicano et al., 2002	RRID:MGI:2182924
Mouse: POMC-Cre: Tg(Pomc1-cre)16Lowl/J	The Jackson Laboratory	Cat#JAX:005965; RRID: IMSR_JAX:005965
Mouse: POMC-eGFP: C57BL/6J-Tg(Pomc-EGFP)1Low/J	The Jackson Laboratory	Cat#JAX:009593; RRID: IMSR_JAX:009593
Mouse: Rosy: B6.129X1-Gt(ROSA)26Sor ^{tm1(EYFP)Cos} /J	The Jackson Laboratory	Cat#JAX:006148; RRID: IMSR_JAX:006148
Mouse: <i>Rptor</i> -Flox: B6.Cg- <i>Rptor</i> ^{tm1.1Dmsa} /J	The Jackson Laboratory	Cat#JAX:013188; RRID: IMSR_JAX:013188
Mouse: <i>Rictor</i> -Flox: <i>Ptprc</i> ^b <i>Thy1</i> ^a <i>Rictor</i> ^{tm1.1Klg} /SjmJ	The Jackson Laboratory	Cat#JAX:020649; RRID: IMSR_JAX:020649
Mouse: <i>CB₁</i> -Flox: <i>Cnr1</i> ^{tm1.2Ltz}	Marsicano et al., 2003	RRID: MGI:3045419
Mouse: POMC-CreER ^{T2} : C57BL/6J-Tg(Pomc-creERT2)	Berglund et al., 2013	N/A
Mouse: Ai6: B6.Cg-Gt(ROSA)26Sor ^{tm6(CAG-ZsGreen1)Hze} /J	The Jackson Laboratory	Cat# JAX:007906; RRID: IMSR_JAX:007906

Oligonucleotides

PCR primers used for mouse genotyping, see Table S5	This paper	N/A
PCR primers used for synthesizing AgRP probe (double FISH)	Allen Brain Atlas	#RP_050419_04_D06
PCR primers used for synthesizing POMC probe (double FISH)	Allen Brain Atlas	#RP_Baylor_102974
PCR primers used for synthesizing POMC probe (triple FISH): Forward: GCAGTGACTAAGAGAGGCCACT Reverse: ATTTAGGTGACACTATAGAAGAGGAC TGCCATCTCCCCACAC	This paper	N/A
PCR primers used for synthesizing Gad67 probe (triple FISH): Forward: GAAAGGGCCAATTCAGTCAC Reverse: ATTTAGGTGACACTATAGAAGAGCTGCC TTCAGTGAGATGGCCTAG	This paper	N/A
PCR primers used for synthesizing vglut2 probe (triple FISH): Forward: TCATTGCTGCACTCGTCCACTA Reverse: ATTTAGGTGACACTATAGAAGAGCC CTGGGATAGTTTGACGTCCA	This paper	N/A

Recombinant DNA

Plasmid: Gq-coupled human M3 muscarinic DREADD (hM3Dq) fused to mCherry	Alexander et al., 2009	N/A
Plasmid: pAAV-Ef1a-DIO-hChR2(H134R)-mCherry-WPRE-pA	Kozorovitskiy et al., 2012	Addgene Plasmid #37082 RRID:Addgene_37082
Plasmid: CAG-DIO rAAV	Atasoy et al., 2008	N/A

Software and algorithms

Adobe Illustrator® CS5	Adobe Systems Software	N/A
AxonpCLAMP 10	Molecular Devices	https://support.moleculardevices.com/s/article/Axon-pCLAMP-10-Electrophysiology-Data-Acquisition-Analysis-Software-Download-Page

(Continued on next page)

Continued

REAGENT or RESOURCE	SOURCE	IDENTIFIER
Database for Annotation, Visualization and Integrated Discovery (DAVID) Bioinformatics Resources 6.7	Dennis et al., 2003	https://david.ncifcrf.gov/
Genepattern 3.9.8	Reich et al., 2006	https://cloud.genepattern.org/gp/pages/login.jsf
HALO	Indica Labs Inc.	https://indicalab.com/halo/
ImageJ	Schneider et al., 2012	https://imagej.nih.gov/ij/
Imaris 8.1.2	Oxford Instruments	https://imaris.oxinst.com/
Prism versions 6 and 8	GraphPad Software	https://www.graphpad.com/scientific-software/prism/
R	R Core Team, 2020	https://www.R-project.org
Other		
34 g blunt NanoFil needle Tip	World Precision Instruments	Cat#NF34BL-2
Cannulas: Single Guide Cannula for Mice	Bilaney Consultants	Cat#C313GS-5/SPC
Cannulas: Dummy Cannula	Bilaney Consultants	Cat#C313DCS-5/SPC
Cannulas: Internal Cannula (injector)	Bilaney Consultants	Cat#C313IS-5/SPC
Cryostat: CM1950	Leica Biosystems	https://www.leicabiosystems.com/histology-equipment/cryostats/leica-cm1950/
Digitizer: Digidata 1440A	Molecular Devices	N/A
Micropipette puller: P-97	Sutter Instrument	https://www.sutter.com/MICROPIPETTE/p-97.html
Micropipettes: borosilicate glass (O.D. 1.5 mm, I.D. 0.86 mm)	Sutter Instrument	https://www.sutter.com/MICROPIPETTE/glass.html
NanoFil syringe 10 μ L	World Precision Instruments	Cat#NANOFIL
Standard rodent diet (Chow)	SAFE [®] Complete Care Competence	Cat#SAFE [®] A03 SP*
UltraMicroPump UMP3 with four channel micro controller SYS-Micro 4	World Precision Instruments	Cat#UMP3-1
Vibratome: VT1200 S	Leica Biosystems	https://www.leicabiosystems.com/histology-equipment/sliding-and-vibrating-blade-microtomes/vibrating-blade-microtomes/leica-vt1200-s/

RESOURCE AVAILABILITY

Lead contact

Further information and requests for resources and reagents should be directed to and will be fulfilled by the Lead Contact, Daniela Cota (daniela.cota@inserm.fr). All main resources and reagents are listed in the [Key resources table](#).

Materials availability

AAV1/2-DIO-hM3Dq-mCherry and AAV1/2-DIO-hChR2-mCherry correspond to virus n^o14 and n^o36 from our lab stock, respectively, and are available upon request.

Data and code availability

The datasets used in this article are publicly available (GEO accession number: GSE74672) ([Romanov et al., 2017](#)).

This paper does not report original code.

Any additional information required to reanalyze the data reported in this paper is available from the lead contact upon request.

EXPERIMENTAL MODEL AND SUBJECT DETAILS

Mice

Male mice, aged 7-16 weeks, were housed individually in standard plastic rodent cages, maintained at 22 \pm 2 $^{\circ}$ C on a 12-h light-dark cycle (lights off at 1300 h) with *ad libitum* access to pelleted chow (Standard Rodent Diet A03, SAFE, France; 3.236 kcal/g; 13.5%

calories from lipids, 25.2% calories from proteins and 61.3% calories from carbohydrates) and water, unless otherwise specified. Cages and enrichment (cotton nest) were changed weekly. Number of animals for each experiment is detailed in the figure legends. Mice were allocated to experimental groups taking care to have similar body weight per group before the start of the experiments.

C57BL/6J mice (Janvier, France or Charles River, UK), *CB₁*-KO mice (Marsicano et al., 2002), POMC-Cre mice [Tg(Pomc1-cre)16Lowl/J, JAX Stock #005965, The Jackson Laboratory, USA], POMC-eGFP mice (Jax Stock #009593, The Jackson Laboratory), POMC-YFP mice, POMC-*Rptor*-KO, POMC-*Rictor*-KO, POMC-*CB₁*-KO, and their control littermates as well as POMC-CreER^{T2}-Ai6 were used. POMC-YFP mice were obtained by crossing POMC-Cre mice with Rosy mice [B6.129X1-Gt(ROSA)26Sortm1(EYFP)Cos/J, JAX Stock #006148, The Jackson Laboratory]. POMC-*Rptor*-KO were generated by crossing POMC-Cre mice with *Rptor*-Flox mice (B6.Cg-Rptortm1.1Dmsa/J, JAX Stock #013188). POMC-*Rictor*-KO were obtained by crossing POMC-Cre mice with *Rictor*-Flox mice (Rictortm1.1Klg/SjmJ, JAX Stock #020649). POMC-*CB₁*-KO were generated by crossing POMC-Cre mice with *CB₁*-Flox mice (Marsicano et al., 2003). Inducible POMC-CreER^{T2}-Ai6 mice were generated by crossing POMC-CreER^{T2} mice (Berglund et al., 2013) with Ai6 mice (B6.Cg-Gt(ROSA)26Sortm6(CAG-ZsGreen1)Hze/J, JAX stock #007906). The constitutive *CB₁*-KO strain was generated and genotyped as previously described (Marsicano et al., 2002). New conditional KO lines were generated following a three step backcrossing method (Bellocchio et al., 2013). All lines were in a mixed genetic background. All animals used in experiments involving mutant mice were littermates. We have previously characterized POMC-*Rptor*-KO mice and POMC-*CB₁*-KO mice (Haissaguerre et al., 2018; Mazier et al., 2019). Effective Cre-mediated deletion of *Rictor* in POMC neurons was assessed by immunohistochemistry.

All experiments were conducted in strict compliance with the European Union recommendations (2013/63/EU) and were approved by the French Ministry of Higher Education, Research and Innovation (animal experimentation authorization n° 3309004) and the local ethical committee of the University of Bordeaux (DIR1354; APAFIS13232). For the triple FISH studies (see further below), no regulated procedures under the Animals (Scientific Procedures) Act 1986 were carried out on the animals used and the studies was reviewed by the University of Cambridge Animal Welfare and Ethical Review Body (AWERB).

METHOD DETAILS

PCR for mouse genotyping

PCR on tail biopsies was performed as in (Bellocchio et al., 2013) by using specific primers (see Table S5 in Supplemental Information).

AAV vectors for hM3Dq and channelrhodopsin-2 (ChR2) expression

Gq-coupled human M3 muscarinic DREADD (hM3Dq) fused to mCherry (Alexander et al., 2009), provided by Brian L. Roth (University of North Carolina, Chapel Hill, NC, USA) was subcloned in a CAG-DIO rAAV vector for Cre-dependent expression (Atasoy et al., 2008) using standard molecular biology techniques. AAV-DIO-hChR2-mCherry was generated using pAAV-Ef1a-DIO-hChR2(H134R)-mCherry-WPRE-pA plasmid as backbone (gift from Bernardo Sabatini; Addgene plasmid # 37082; Kozorovitskiy et al., 2012). Vectors used were of an AAV1/AAV2 mixed serotype, and were generated by calcium phosphate transfection of HEK293T cells and subsequent purification as described (Monory et al., 2006).

Stereotaxic surgery

Mice were anesthetized with a mixture of ketamine (100 mg/kg, ip) and xylazine (10 mg/kg, ip), placed in a stereotaxic holder (David Kopf Instruments, USA) and implanted with a cannula in the lateral cerebral ventricle (coordinate AP/DV/ML = -0.5/-2.1/-1.2 mm). Cannula placement was verified by administering 5 μg of neuropeptide Y (NPY) (Phoenix Pharmaceuticals Inc., France) in 0.01 M PBS (pH 7.4) and assessing subsequent food intake (Brown et al., 2006).

Stereotaxic virus injection

AAV vectors (500 nL) were bilaterally infused into the ARC (coordinate AP/DV/ML = -1.5/-5.5/ ± 0.2 mm; infusion speed = 100 nL/min; UltraMicroPump UMP3 with SYS-Micro4 Controller, WPI, USA) using a NanoFil syringe (10 μL) with a 34G blunt needle (85 μm internal tip diameter) (WPI, USA). AAV-DIO-hM3Dq-mCherry vectors were injected into the ARC of POMC-Cre^{+/+} (thereafter named POMC-ARC^{hM3Dq} mice) and of POMC-Cre^{-/-} mice (thereafter named POMC-ARC^{hM3Dq}-control mice). Mice were then implanted with cannulas into the lateral ventricle as detailed above. Mice were used for the behavioral studies after at least 4 weeks from the intra-ARC AAV administration. For optogenetic electrophysiology studies, 5-weeks old POMC-Cre^{+/+} mice were stereotaxically and bilaterally injected with an AAV-DIO-hChR2-mCherry virus and used for electrophysiology 4-5 weeks after the intra-ARC AAV administration.

Food intake studies

Drugs preparation

Rapamycin (RAPA, Sigma Aldrich), rimonabant (NIMH Chemical Synthesis and Drug Supply Program, USA) and picrotoxin (Ptx, Sigma-Aldrich), were dissolved in DMSO, the clozapine-N-oxide (CNO, Sigma-Aldrich) was dissolved in saline.

Recording of basal food intake

Before undergoing pharmacological studies, 24h basal, unstimulated, food intake was recorded over several days in POMC-*Rictor*-KO, POMC-*CB₁*-KO, and their control littermates. Unstimulated food intake in POMC-*Rptor*-KO has been previously described in (Haissaguerre et al., 2018).

Fasting-induced food intake studies

24h fasted mice received an icv injection of RAPA (25 μ g in 1 μ L DMSO) or its vehicle, which were administered 4h before dark onset. The same protocol was followed when rimonabant (5 μ g in 1 μ L DMSO), Ptx (0.03 μ g in 1 μ L DMSO), or CNO (1 mg/kg in saline, ip) were combined with RAPA. Rimonabant and Ptx were simultaneously administered icv with RAPA; CNO or its vehicle were administered 15 min before the icv administration of RAPA or its vehicle. Food was returned immediately after the drugs injections. Whenever possible the same animals belonging to the same genotype underwent the different treatments within the same experiment. Animals showing sign of stress or malaise during the experiments were removed from further analysis.

Ptx dose-responses

The Ptx dose-response was carried out in 24h fasted C57BL/6J mice that received Ptx (0.03, 0.06 or 0.09 μ g/ μ L in DMSO, icv) 4 h before dark onset. Food was returned immediately after the drugs injections.

Immunohistochemistry (IHC)

Tissue sample collection

Mice were deeply anesthetized using pentobarbital given ip and then perfused transcardially with ice-cold PBS, pH 7.4, followed by 4% paraformaldehyde (PFA, Sigma-Aldrich) in PBS with 0.2% picric acid. Brains were extracted and postfixed in 4% PFA overnight at 4°C, then cryoprotected with 30% sucrose in PBS at 4°C. Coronal sections (30 μ m) were cut with a cryostat (CM1950, Leica, Germany), collected and stored in antifreeze solution (30% ethylene glycol, 20% glycerol in PBS) at -20°C until further used.

Double-labeling IHC

Brain sections from POMC-*Rictor*-KO and their control littermates were processed for the co-localization of rictor and POMC. Sections were first incubated with 10% normal goat serum (Agilent Technologies) and then with rabbit anti-rictor antibody (1:1000, Bethyl Laboratories, Inc., USA) overnight at 4°C. The next day sections were washed in PBS and incubated for 1h with A647-conjugated secondary goat anti-rabbit antibody (1:500, Cell Signaling). Sections were washed in PBS and incubated with Goat Fab Fragment Anti-Rabbit IgG (1:100, Jackson ImmunoResearch Laboratories, USA) to avoid cross-reactivity. Sections were then washed in PBS and blocked with 10% normal goat serum (Agilent Technologies) and incubated with rabbit anti-POMC antibody (1:2000; Phoenix Pharmaceuticals) overnight at 4°C. The next day sections were washed in PBS and incubated for 1h with A488-conjugated secondary goat anti-rabbit antibody (1:500, Cell Signaling). Sections were then mounted with ProLong gold mountant and coverslipped.

Evaluation of chemogenetic activation of POMC neurons

Free-fed POMC-ARC^{hM3Dq} mice received a single injection of CNO (1 mg/kg, ip) or its vehicle 90 minutes before sacrifice and expression of c-Fos and phosphorylated S6 ribosomal protein (p-S6) in mCherry-expressing POMC neurons was evaluated. Collected sections from perfused brain samples were first incubated with 10% normal donkey serum (Jackson ImmunoResearch Laboratories) and then with goat anti-c-Fos antibody (1:250; Santa Cruz Biotechnology, USA) overnight at 4°C. The next day sections were washed in PBS and incubated for 1h with A488-conjugated secondary donkey anti-goat antibody (1:500, Thermo Fisher Scientific). Sections were then washed in PBS and blocked with 10% normal goat serum (Agilent Technologies) and subsequently incubated with rabbit anti-p-S6 ser240/244 antibody (1:200; Cell Signaling) overnight at 4°C. The next day sections were washed in PBS and incubated for 1h with A647-conjugated secondary goat anti-rabbit antibody (1:500, Cell Signaling).

Triple-labeling IHC

Brain sections from 24-h fasted and 90 min refed C57BL/6J mice icv treated with RAPA or its vehicle were processed for the expression of c-Fos and p-S6 in POMC neurons. Sections were first incubated with 10% normal donkey serum (Jackson ImmunoResearch Laboratories) and then with goat anti-c-Fos antibody (1:250; Santa Cruz Biotechnology) overnight at 4°C. The next day sections were washed in PBS and incubated for 1 h with A594-conjugated secondary donkey anti-goat antibody (1:500, Thermo Fisher Scientific). Sections were then washed in PBS and blocked with 10% normal goat serum (Agilent Technologies) and then incubated with rabbit anti-p-S6 antibody (1:200; Cell Signaling) overnight at 4°C. The next day sections were washed in PBS and incubated for 1 h with biotinylated goat anti-rabbit IgG secondary antibody (1:400, Vector Labs), followed by washes and 1 h of amplification with an avidin-biotin complex (Vectastain Elite ABC kit, Vector Labs). The sections were then washed and incubated with a Fluorescein-conjugated streptavidin (1:400, Vector Labs). Finally, sections were washed in PBS and incubated with Goat Fab Fragment Anti-Rabbit IgG (1:100, Jackson ImmunoResearch Laboratories) to avoid cross-reactivity. Sections were then washed in PBS and blocked with 10% normal goat serum (Agilent Technologies) and then incubated with rabbit anti-POMC antibody (1:2000, Phoenix Pharmaceuticals) overnight at 4°C. The next day sections were washed in PBS and incubated for 1 h with A647-conjugated secondary goat anti-rabbit antibody (1:500, Cell Signaling). Sections were then mounted with ProLong gold mountant and coverslipped.

Quantification of the immunohistochemical signal

Fluorescent images were acquired with a confocal microscope (SP8-STED, Leica, Germany), corrected for brightness and contrast, and analyzed using ImageJ (Schneider et al., 2012). For illustration purposes, representative images have been subjected to enhancements, including background subtraction as well as brightness and contrast adjustment. For multiple color images, each

channel has been processed independently. Images from different conditions were modified identically, unless otherwise specified in the figure legend (Figure S1D).

Fluorescent *in situ* hybridization (FISH)

Double FISH

Brain sections from perfused brains samples of 16 weeks-old POMC-CreER^{T2}-Ai6 mice, which had received at 8 weeks of age 150mg/kg of tamoxifen for 5 consecutive days by oral gavage, were used to assess possible co-expression of *Agrp* and *Pomc* mRNA. Digoxigenin-labeled riboprobe against mouse *Agrp* (AgRP-DIG, Allen Brain Atlas, #RP_050419_04_D06) and fluorescein-labeled riboprobe against mouse *Pomc* (POMC-FITC, Allen Brain Atlas, #RP_Baylor_102974) were prepared as in (Marsicano et al., 2002). Free-floating sections were treated with 0.2M HCl then acetylated with 0.25% acetic anhydride in 0.1 M triethanolamine, pH = 8.0 for 10 min. Between all steps, sections were rinsed in PBS with 0.01% diethylpyrocarbonate (DEPC). AgRP-DIG and POMC-FITC probes were dissolved 1:1000 in hybridization solution (50% deionized formamide, 20mM Tris at pH = 8.0, 300mM NaCl, 5mM EDTA, 10% dextran sulfate, 1X Denhardt's solution, 0.5mg/mL tRNA, 0.2mg/mL acid-cleaved carrier DNA from salmon's sperm, 200mM DTT dissolved in water containing 0.01% DEPC) and heated at 90°C for 5min. After hybridization overnight at 70°C, sections were washed at 65°C with increased stringency buffers (5X SSC for 5min, 2X SSC+50%Formamide, 1X SSC+50%Formamide and 0.1X SSC for 30min each, with 0.1% Tween20 added to each buffer). After blocking 1h in TNB blocking buffer (AkoyaBiosciences, prepared as per manufacturer's instructions), sections were incubated overnight at 4°C in anti-DIG-POD antibody (1:1500, Roche) in TNB. The revelation was made using TSA-Cy3 kit (1:100, 30min, AkoyaBiosciences). After quenching the peroxidase with 3% H₂O₂ in PBS (30min) and 0.2M HCl treatment (20min), sections were incubated in anti-FITC-POD antibody (1:1500, Roche) in TNB for 2h and the revelation made using TSA-FITC kit (1:100, 30min, AkoyaBiosciences).

Triple FISH

C57BL/6J mice were killed by an overdose of pentobarbital. The brains were removed, instantly embedded in OCT Embedding Medium (Thermo Scientific) and stored at -80°C. 10 μm thick coronal sections of the entire ARC were prepared on a Leica CM1950 Cryostat. One section every 100 μm was stained and analyzed from each animal. The following primers were used for FISH antisense probe production: *Pomc* forward GCAGTGACTAAGAGAGGCCACT, *Pomc* reverse ATTTAGGTGACACTATAGAAGAGGACTGC CATCTCCCCACAC; *Gad1* (hereafter referred to as *Gad67*) forward GAAAGGGCCAATTCAGTCAC, *Gad67* reverse ATTTAGGTGACACTATAGAAGAGCTGCCTTCAGTGAGATGGCCTAG; *Slc17a6* (hereafter referred to as *Vglut2*) forward TCATTGCTGCACTCGTC CACTA, *Vglut2* reverse ATTTAGGTGACACTATAGAAGAGCCCTGGGATAGTTTGAGTCCA. Reverse primers included a SP6 recognition sequence. A hypothalamic mouse RNA library was reverse transcribed into a cDNA library and DNA templates for the relevant transcripts were obtained via PCR using the above primers. Subsequently, these templates were *in vitro* transcribed into antisense RNA probes using MAXIscript SP6 *In Vitro* Transcription Kit (Thermo Fischer Scientific). 35% of the UTP in each reaction was replaced with either Fluorescein-12-UTP (Roche), Digoxigenin-11-UTP (Roche) or DNP-11-UTP (PerkinElmer) for *Pomc*, *Vglut2* and *Gad67* probe production, respectively. For FISH, the following antibodies and tyramide solutions were used: Anti-Fluorescein-POD Fab fragments (Roche), Anti-Digoxigenin-POD Fab fragments (Roche) and Anti-DNP HRP Conjugate (PerkinElmer) as well as Cyanine 3 Tyramide Reagent and Cyanine 5 Tyramide Reagent and Fluorescein Tyramide Reagent (all AkoyaBiosciences), respectively. Briefly, cryosections were fixed in 4% PFA, washed in PBST and 0.1 M TEA and acetylated, washed again in PBST, and in 5x SSC/50% formamide at 65°C. They were pre-hybridized in prehybridization buffer (50% formamide, 5X SSC, 0.05mg/mL Heparin, 0.5mg/mL tRNA, 0.1% Tween20 dissolved in RNase-free water) for 30 min at 65°C and incubated with hybridization buffer (prehybridization buffer with 10% dextran sulfate) containing all three antisense RNA probes overnight at 65°C. Following washes in 5x SSC, 1x SSC/50% formamide, 2x SSC and 0.2x SSC at 65°C, slides were rinsed with Maleic Acid Buffer with Tween20 (MABT), incubated with one of the above antibodies for 1h, washed with MABT again and developed with one of the above tyramide solutions for 20 min in the dark. Slides were washed with PBST and the remaining enzyme activity of the antibody quenched with 3% H₂O₂ in PBS for 30 min and subsequent citrate buffer at 95°C for 10 min. The antibody and tyramide incubation steps and the quenching procedure were repeated twice with the remaining antibodies and tyramide solutions. Finally, slides were washed several times in MABT, counterstained with DAPI in PBST and mounted with Aqua-Poly/Mount (Polysciences). All steps were carried out at room temperature unless stated otherwise.

Triple FISH image acquisition and analysis

Whole-slide images were acquired on an Axio Scan.Z1 (Zeiss). Image analysis and cell counts were obtained manually in the HALO software (Indica Labs Inc.). Analysis thresholds were applied before images were taken. Brightness and contrast were subsequently modified to facilitate signal visibility. A schematic image of each analyzed coronal brain section was created using Adobe Illustrator CS5 (Adobe Systems Software). For each POMC neuron, its distance to the ventricle and the subpopulations it belonged to was extracted from these schematic images by a custom-written Python script (Graham N. Stratton).

Hypothalamic neuropeptides assays

Hypothalami from 24h fasted or 2h refed C57BL/6J mice, treated icv with RAPA or its vehicle, were dissected, flash frozen, and stored at -80°C until analysis. Samples were extracted in 0.1N HCl and assayed for α-MSH and β-EP by RIA as in (Savontaus et al., 2004). ACTH RIA was performed as in (Papadopoulos and Wardlaw, 1999). ELISA for POMC protein was performed with reagents provided by Dr. Anne White at the University of Manchester (Tsigos et al., 1993). Data are expressed versus mg of protein.

Endocannabinoid measurements

Hypothalamus, hippocampus and cortex of 24h fasted or 1h refed C57BL/6J mice, treated icv with RAPA or its vehicle, were dissected, flash frozen, and stored at -80°C until analysis. Measurements of AEA and 2-AG were performed as in (Gatta-Cherifi et al., 2012). Endocannabinoids content was expressed versus mg of tissue.

Single-cell RNA sequencing analysis

RNA-seq data on *Pomc*-expressing neurons (≥ 2 mRNA copies per cell) were extracted from our publicly available dataset on hypothalamic neurons obtained from 2-4 weeks old C57BL/6N mice (GEO accession number: GSE74672 (Romanov et al., 2017)). We evaluated the distribution of cells expressing *Pomc* transcripts in the hypothalamus through public databases on *in situ* mRNA hybridization (Allen Brain Atlas, Mouse Brain, experiments 2493 and 2494) and noted highly specific *Pomc* expression in the ARC. This validates that *Pomc*-expressing neurons in our single-cell RNA-seq dataset originate from the ARC, and can be used for subtype deconvolution. For the validity of our following analysis, we checked cells for outliers using Principal Component Analysis to exclude those neurons coming to the dataset because of the contamination/ectopic *Pomc* gene transcription. Finally, we performed differential gene expression profiling of *Pomc*⁺ neurons by using Genepattern 3.9.8 [(Reich et al., 2006); <https://cloud.genepattern.org/gp/pages/login.jsf>] with the “ComparativeMarkerSelection” and “ExtractComparativeMarkerResults” modules. Data were then rendered into heatmaps (HeatMapImage module) for maximum visual clarity. The Database for Annotation, Visualization and Integrated Discovery (DAVID) Bioinformatics Resources 6.7 (Dennis et al., 2003) was used to identify the genes that had statistically significant differences in expression among the different POMC neuron subpopulations (Huang et al., 2009). To interpret our data, we used the «Functional annotation chart» tool. This tool associates gene ID with a biological term which belongs to one out of the 40 annotation categories available in DAVID, including Gene Ontology terms and Kyoto Encyclopedia of Genes and Genomes (KEGG) pathways. This extended annotation coverage increases the analytic power by allowing investigators to analyze their genes from many different biological aspects in a single space. Each functional annotation was associated with an enrichment score, which depended on the distribution of the enrichment (p values) of each gene. A good enrichment score was obtained when most of genes had good p values. This score is a relative score instead of a statistical probability with a minimum and a maximum value. This means that enrichment scores could be considered only together, by comparing them.

Electrophysiology

Brain slices preparation

Acute coronal brain slices were prepared from 8 to 12 week-old mice expressing YFP or Chr2 coupled to mCherry selectively in POMC neurons or from POMC-*CB₁*-KO and their control littermates. For the analysis of direct or indirect effects of RAPA on POMC neurons, acute coronal brains sections were prepared from 8 weeks-old POMC-eGFP mice. Animals were anesthetized with isoflurane, the brain extracted and immediately placed in an ice-cold oxygenated cutting solution (in mM: 180 Sucrose, 26 NaHCO₃, 11 Glucose, 2.5 KCl, 1.25 NaH₂PO₄, 12 MgSO₄, 0.2 CaCl₂, saturated with 95% O₂–5% CO₂). Slices were obtained using a vibratome (VT1200S Leica, Germany) and transferred into a 34°C bath of oxygenated aCSF (in mM: 123 NaCl, 26 NaHCO₃, 11 Glucose, 2.5 KCl, 1.25 NaH₂PO₄, 1.3 MgSO₄, 2.5 CaCl₂; osmolarity 310 mOsm/l, pH 7.4) for 30 minutes and then cooled down progressively till room temperature (RT; 23-25°C) in oxygenated aCSF. After a 45 min recovery period at RT, slices were bisected by cutting along the third ventricle axis. The hemi-slice was anchored with platinum wire at the bottom of the recording chamber and continuously bathed in oxygenated aCSF (32-34°C; 2ml/min) during recording.

Patch electrodes were pulled (micropipette puller P-97, Sutter instrument, USA) from borosilicate glass (O.D. 1.5 mm, I.D. 0.86 mm, Sutter Instrument) to a resistance of 2-4 mΩ.

The pipette internal solution contained [in mM: 125 potassium gluconate, 5 KCl, 10 HEPES, 0.6 EGTA, 2 MgCl₂, 7 Phosphocreatine, 3 adenosine-5'-triphosphate (magnesium salt), 0.3 guanosine-5'-triphosphate (sodium salt) (pH adjusted to 7.25 with KOH; osmolarity 300 mOsm/l adjusted with d-Mannitol; liquid junction potential –14.8mV corrected on the data presented)]. Electrophysiological data were recorded using a Multiclamp 700B amplifier (Molecular devices, UK), low-pass filtered at 4 kHz and digitized at 10Hz (current clamp) or 4 Hz (voltage clamp) (Digidata 1440A, Molecular devices, UK). Signals were analyzed offline (pClamp 10, Molecular devices, UK).

Evaluation of WIN effect on mIPSC on PVN parvocellular neurons of POMC-CB₁ mice

Parvocellular neurons were differentiated from magnocellular neurons immediately after patch rupture by preliminary electrophysiological analysis. Indeed, when submitted to a depolarizing current magnocellular neurons exhibit a large transient outward rectification, not found in parvocellular neurons (Luther and Tasker, 2000). Then cells were switched in voltage clamp ($V_h = -70$ mV). Miniature GABAergic transmission was pharmacologically isolated using a mix of NBQX (10 μM), APV (50 μM) and tetrodotoxin (TTX, 1 μM). Note that as a control, few cells were perfused with a GABAA selective antagonist (picrotoxin, 100 μM) at the end of the experiment to fully block miniature transmission. To challenge the CB₁ receptor, the selective agonist (WIN55-212, 5 μM) was added. For statistical analysis, miniature events frequency and amplitude during the last 4 minutes of baseline were compared to the same parameters after 10 minutes of drug perfusion (4 minutes also).

Evaluation of RAPA and leptin effect on POMC neurons firing

Fluorescent POMC-YFP neurons were identified onto 250 μm thick slices obtained from 8-12 weeks old male POMC-YFP mice, using fluorescence/infrared light (pE-2 CoolLED excitation system, UK). Neurons action potential firing was monitored in whole-cell current-clamp recording configuration. For each recorded neuron, membrane potential (E_m), membrane capacitance (C_m) and

membrane resistance (R_m) were collected right after cell opening. After a 10 min baseline, RAPA (200 nM) or leptin (200 nM, National Hormone and Peptide Program, USA) was added in the bath for 20 minutes. For the analysis, considering the variability of the POMC neurons basal firing, the significance of RAPA-induced changes or of leptin-induced changes in action potential firing was assessed by comparing the firing rate before and during RAPA or leptin application (bin size of 10 s), respectively, using normalization via Z-score transformation of individuals' instantaneous frequencies values (Courtin et al., 2014). Z-score values were calculated by subtracting bin average instantaneous frequencies to the average baseline instantaneous frequency established over at least 120 s preceding RAPA or leptin application and by dividing the difference by the baseline standard deviation. Both RAPA and leptin responsiveness were evaluated by comparing the firing rates (Z-score) obtained during the 120 s before the drug application with the ones obtained 4 min after the drug application. Neurons with at least 5 significant positive or negative z-score bins (z-score $> \pm 1.96$, $p < 0.05$) after RAPA or leptin application were considered as drug-responsive neurons.

For the determination of the direct versus indirect effect of RAPA on POMC neurons, after 5 minutes of baseline, a cocktail of GABA (gabazine (5 μ M), picrotoxin (100 μ M)) and glutamate [cyanquinoxaline (CNQX), 20 μ M] and D-APV (50 μ M)] blockers were perfused for 5 minutes before and during RAPA (200 nM) application. Membrane potential was measured over the last 60 s before and after 5 minutes RAPA application. Change in membrane potential (ΔV_m) strictly above or below 1 mV was used as a cut-off for the determination of RAPA^{act} (> 1 mV), RAPA^{inh} (< 1 mV) and RAPA^{ns} (-1 mV $\leq \Delta V_m \leq 1$ mV). The quantification of change in firing rate frequency could not be used in this specific set of experiments since the application of GABA and glutamate blockers hyperpolarized and silenced most of recorded POMC neurons.

Effect of RAPA on light-evoked POMC to parvocellular neurons neurotransmission

350 μ m slices were prepared from brains of POMC-Cre^{+/+} mice bilaterally injected with an AAV-DIO-hChR2. The aCSF was modified in order to increase the neurotransmission success rate (3 mM Ca²⁺, 0.1 mM Mg²⁺ and 100 μ M 4 aminopyridine). Parvocellular neurons were switched in voltage clamp configuration ($V_h = -70$ mV) and synaptic transmission was evoked with a 5 ms flash of blue light (470 nm, 1-3 mW at 0.03 Hz; pE-2 CoolLED excitation system). Light-evoked glutamatergic or GABAergic transmission was pharmacologically isolated using picrotoxin (100 μ M) or a NBQX/APV mix (10 μ M/50 μ M), respectively. RAPA was added for 20 minutes after at least 10 minutes of stable amplitude light-evoked eEPSCs or eIPSCs. At the end of each experiment, responses were fully blocked using TTX (1 μ M). For statistical analysis, mean eEPSCs or eIPSCs amplitudes during the last 4 minutes of baseline period were compared to the amplitudes obtained in the same cells after 5 minutes of RAPA perfusion.

POMC neuronal type characterization after recording

During recording POMC neurons were filled via passive diffusion of biocytin (0.4% in internal solution, Sigma, France). Afterward, slices were fixed overnight at 4°C in 4% PFA-containing phosphate buffer (PB). After washing (3x15min in PB), slices were permeabilized and saturated for 3h at RT (0.3% triton, 10% bovine serum albumin in PB). Slices were incubated with primary antibody (anti-GAD65/67 made in rabbit, 1/2000, Millipore) for 72h at 4°C. Then the fluorophore-coupled secondary antibody (A647-conjugated secondary goat anti-rabbit antibody, 1:500, Cell Signaling, USA) and a fluorescent streptavidin (AMCA, anti-biotin, 1/1000, Vector laboratories) were applied overnight at 4°C. Slices were mounted with fluoromount and stored at 4°C in the dark. Pictures of POMC cells were captured using a confocal microscope with objective 63X (SP8-STED, Leica) setting fixed acquisition parameters. Sampling rate respected the optic resolution of the system (voxel size: 0.0819x0.0819x0.2985 μ m³) and z axis stacks were processed (around 20 images per cells). Images were acquired separately for each wavelength (blue = 405 nm and far red = 647 nm) and then merged for analysis. Using Imaris 8.1.2 software (Oxford Instruments, Switzerland), POMC cell body volume (default settings for surface reconstruction) and individual GAD65/67 staining spots (0.4 μ m diameters dots, threshold of 3500 pixels set taking into account background signal obtained from staining carried out in the absence of the primary antibody) were automatically reconstructed in 3D. A dedicated analysis module allowed making a clear distinction between the GAD65/67 spots located around the cell and the ones present within the cell body of the POMC neuron.

QUANTIFICATION AND STATISTICAL ANALYSIS

Statistical analyses were performed using Prism, versions 6 and 8 (Graphpad, USA). All values, unless stated otherwise in the figure legends, are reported as means \pm SEM. Data were analyzed by unpaired or paired Student's t tests, one-way or two-way ANOVAs, as appropriate. Repeated-measures (RM) for matched individuals were used when same animals underwent different treatments. Significant ANOVAs were followed by Fisher Least Significant Difference (LSD) post hoc test. A Kruskal-Wallis test followed by Dunn's post-test was used to assess differences in the distance to the ventricle across the different POMC subpopulations. To describe rostro-caudal changes in the distance to the ventricle for each subpopulation, linear regression analysis was performed using the software R (R Core Team, 2020) followed by ANOVA. Single-cell RNA-seq data for the various *Pomc*⁺ cells subgroups was analyzed using Student's t test on log-transformed mRNA copy data. $p < 0.05$ denote statistical significance. Detailed statistical analysis is provided in Tables S3 and S4.